

Wavelength Effects on *In Vivo* Confocal Scanning Laser Microscopy

A Thesis

Submitted to the Faculty

of

Drexel University

by

Michael A. Luedtke

In partial fulfillment of the

requirements for the degree

of

Masters of Science in Biomedical Engineering

November 2007

© Copyright 2007

Michael A. Luedtke. All Rights Reserved

Dedication

This thesis is dedicated to my wife (our son Owen's mother) Kathryn for her patience, support and love.

Acknowledgements

I would like to acknowledge the following institutions and individuals for their support (with equipment, software) and guidance throughout the entire research process.



School of Biomedical Engineering, Science & Health Systems



Elisabeth Papazoglou Ph.D.

Linda Zhu



Nikiforos Kollias Ph.D.

Yang Liu Ph.D.

Sheng-Hao Tseng Ph.D.

Greg Payonk Ph.D.



Jay Eastman Ph.D.

William Fox

Zach Eastman



Memorial Sloan-Kettering
Cancer Center

Milind Rajidashka Ph.D.

Dan Geareau Ph.D.

Table of Contents

	Page
Table of Contents.....	vi
List of Tables	viii
List of Figures	ix
Abstract.....	xiii
Introduction	2
Skin and its Structure	3
Optical Properties of Healthy Skin	5
Endogenous Skin Chromophores	7
Confocal Scanning Laser Microscopy Theory	8
Axial Resolution, Lateral Resolution and Point Spread Function	13
Factors Affecting SCLM	17
Optical Variability	18
Aberrations.....	18
Immersion Media.....	19
Hypothesis	21
Description of Experimental Procedure.....	22
Microscope Characterization	22
Point Spread Function Measurement	25
Spatial Calibration of the Microscope	26
Optical Skin Phantom Imaging	26
Human Measurement Study with Different Immersion Media	27

Results	29
Microscope Characterization and Modeling	29
Phantom Measurement with Different Laser Wavelengths	32
Human Skin Study: Measurements at Three Wavelengths	34
Discussion	38
Microscope Characterization	38
Pinhole Size	38
Optics	39
Scattering	40
Optical Phantom Experiments	41
Human Study Experiments	43
Consistent Location of Images Across Wavelengths	43
Skin Wavelength Dependent Observations	44
Conclusions	46
Recommendations	48
References	50
Appendix A – IDL code used for normalizing confocal images as a function of depth analysis	52
Appendix B – MATLAB code used for enhanced normalized intensity analysis as a function of depth	61
Appendix C -- Subject informed consent required for J&J CPPW clinical study.	65
Appendix D	71

List of Tables

Table 1 – Different endogenous chromophores within skin at wavelengths of interest. [7-9].....	8
Table 2 – Immersion media, their indices of refraction and skin features best imaged with these substrates.	20
Table 3 – Table of calculated theoretical axial resolution and theoretical lateral resolution (from Eq1 and Eq2 respectively) as well as the measured FWHM from the different wavelength microscopes, indicating optical section thickness. Also note- the pinhole size allows for 3 resels in <i>in vivo</i> CSLM. This is evident in the actual measured FWHM values. The actual lateral resolution is spatially calibrated across units so is not accounted for with an actual measurement.	31

List of Figures

- Figure 1 – (Left) Illustration of skin and its different tissue layers. The top is the epidermis, next is the reticular and papillary dermis and at the base is the subcutaneous fat. (Right) Illustration of the extra cellular matrix as well as all of the microstructure present within the papillary and reticular dermis.[4]4
- Figure 2 -- (Left) Illustration of the multiple scattering events as photons progress through the skin. (Right) Graphical representation of penetration depth (um) as a function of wavelength in bloodless dermis. Note the lower penetration at shorter wavelengths of light due to higher indexes of scattering and order of magnitude increase at longer wavelengths. These figures only consider scattering and do not consider the absorption. CSLM allows visualization of single scattering events.[7]6
- Figure 3 – Illustration of amount of incident photons with wide field and point source illumination. On the left the wide amount of light and photons that are allowed to be viewed in wide field conventional light microscope (A) and are illustrated on the right (B) the point source principle of the confocal microscopy is illustrated.[11].....9
- Figure 4 – Figure of confocal light properties, as they are observed through a conventional light microscope (1), using a pinhole with the conventional microscope (2) and using a pinhole and point source illumination (3). Figure and captions extracted directly from cited source.[11]..... 11

- Figure 5 – The above model represents changes in index of refraction and the subsequent bending of a ray of light as it enters the skin. Figure 5 fully extracted from source. [6]. 12
- Figure 6 – 6A is a 3D example of a single theoretical resel. The thin red line in 6A is the 2D representation of a cross-section in a the narrow Gaussian distribution in 6C. The full width at half maximum of the measured intensity is the theoretical optical section. 6B is a simple skin illustration of a coherent laser point source in it to illustrate what typically happens to a point source illuminating the skin. Note pink bar and the subsequent cross section in 6C. 6C is a 2D representation of the cross section represented in red and pink for the theoretical and measured points spread functions respectively. 6A, 6B, 6C were compiled and edited and were fully extracted from the following cited websites [14-16]. 14
- Figure 7 – Effect of pinhole size “d” in microns on point spread function (PSF). Note as pinhole widens (d increases), the subsequent PSF is broader and the FWHM also increases. This illustrates that the focal volume increases in size as the pinhole size increases. 16
- Figure 8 – Image of the commercially available scanning laser confocal microscope the Lucid Vivascope 1500. Current standard wavelength is 830nm and experimental wavelengths used were 785nm and 405nm for their ability to do both reflectance mode imaging in addition to fluorescence mode imaging. Note, these are fluid immersion objectives and both oil and water objectives were used to see if there was a significant difference in

resolution between the microscopes. NOTE example of tissue ring and coverslip mechanism that attaches microscope to human skin is a part of the optical design and optical path of the microscope (Images courtesy of Lucid Inc.).....23

Figure 9 – Point Spread Function characterization of the microscopes. Only 785nm and 404nm are displayed on this chart to highlight the size differences in the FWHM of the PSF.30

Figure 10 – Data presented using 6 replicate stacks on the optical skin phantom with oil immersion. Note- the data are highly reproducible and there is a significant increase (40% at the maximum value) of the 830nm data compared to the 785nm data.....32

Figure 11 – This figure compares measurements of the same optical skin phantom in the same location with the 405 microscope and different immersion media. No direct comparison was made among all wavelengths because different objectives were used as well as different coatings. Note that intensity in air is higher than in oil or water. Note that the surface intensity of the water is higher, but the subsurface signal intensity on the oil measurements increases as a function of depth.....33

Figure 12 – Normalized intensity as a function of depth for subject J-N stack 01 (Images in Appendix D). These data are representative of the apparent change in normalized intensity of the confocal image signal as a function of depth. Note there is a higher overall measured signal with the 785nm confocal images. Also note there is an intensity increase with the 405nm

around a depth of 45um, corresponding to the DE junction. This is due to the papillary collagen measured within the dermal papillae.....35

Figure 13 -- Normalized intensity as a function of depth for subject PAR stack 03.

These data are representative of the apparent change in normalized intensity of the confocal image signal as a function of depth. Also note there is an intensity increase with the 405nm around a depth of 45um, corresponding to the DE junction. This is due to the papillary collagen measured within the dermal papillae.36

Figure 14 -- Normalized intensity as a function of depth for subject SKO stack 01.

These data are representative of the apparent change in normalized intensity of the confocal image signal as a function of depth. Note there is a monotonic decrease in the 405nm signal around 45um, at the DE junction. This is due to the presence of melanin measured within the dermal papillae at the 830 and 785 wavelengths.....37

Figure 15 – On left, a 830nm CSLM image with 100um pinhole. On right, a 405nm CSLM image with a 35um pinhole. Notice the sharper delineation of the cells in the 405 image. Both images illustrate the topographical variations within one optical section. There is more variability in depth between the 830nm than there is within the 405 due to the larger optical section.40

Abstract
Wavelength Effects on *In Vivo* Confocal Scanning Laser Microscopy

Michael A. Luedtke

Elisabeth Papazoglou

The ability to optically section live biological tissue *in vivo* with laser light and observe reflections from single scattering events is made possible by *in vivo* confocal scanning laser microscopy (CSLM). In this thesis the effects of using CSLM at different wavelengths to image *in vivo* human skin are reported and analyzed. Upon changing the wavelength of incident light, differences are observed while certain features are maintained. This work attempts to deconvolute differences due to wavelength artifacts from differences revealing important skin microstructure. To illustrate the differences due to the optical set up and wavelength changes, *in vitro* experiments were developed to characterize and model the instrumentation and tissue samples imaged. To further review and illustrate the differences in wavelengths a human test was conducted with 8 subjects to determine qualitative and quantitative differences observed at 405nm, 785nm and 830nm wavelengths from different CSLMs on live human tissue. From these experiments it was found that differences do exist among the selected wavelengths. This was surprising due to the proximity of the near

infrared 785nm and 830nm wavelengths. Future work using 405nm, 785nm, and 830nm lasers on a single CSLM with identical optics in a single experimental setup will enable confirmation of our findings. In conclusion the laser wavelength used in CSLM is important even in reflectance imaging to properly understand and resolve different biological structures within human skin.

Introduction

Reflectance mode confocal scanning laser microscopy (CSLM) is a method that enables microscopic observations of thick samples by means of optical sectioning. This thesis discusses primarily the *in vivo* CSLM as it applies to human skin measurement. The *in vivo* CSLM is a variant of portable confocal microscopy that is configured for the best visualization of skin *in situ* because it allows for a non-invasive optical biopsy without performing a conventional invasive punch biopsy. *Ex vivo* confocal applications utilize a fixed tabletop microscope that is not portable, is anchored to a fixed location and is highly configurable for different applications.

Human skin is a very complicated inhomogeneous structure with many endogenous chromophores, both scatterers as well as absorbers, with two major divisions being the epidermis and the dermis. While biological *in vivo* CSLM is limited to the epidermis and top layers of the dermis it enables accurate and precise noninvasive imaging of skin morphology and physiology. Once an image sequence of optical sections is acquired it can be used to generate a three dimensional reconstruction of the upper layers of skin and allows for quantitative and qualitative measures non-invasively.

In the following sections, an introduction to skin and its amazing complexity with regard to optics and optical properties will be presented. Then the theory behind CSLM will be presented as it applies to *in vivo* skin applications and how it relates to the hypothesis proposed by this thesis.

Skin and its Structure

Skin is the one of the largest, most complex and variable human organs. If removed from the body, it would be 1-2m² depending on the size of the individual.[1] The skin we are born with needs to last our entire life, and it adapts and changes to the surrounding environment to provide a protective barrier from the elements. [2, 3]

Skin is comprised of two main layers, the upper is called the epidermis and the lower layer is called the dermis. Subcutaneous fat is found below the dermis and all of these layers make up our largest organ- skin (Figure 1). [4] The epidermis is comprised of cells that progressively get flatter and drier as they migrate, proliferate and differentiate towards the surface of the skin. [5] The stratum corneum is the outermost surface layer and is comprised of very flat, dry, and dead cells that are about to be desquamated as new cells proliferate from the layers below. [2] Just below the stratum corneum are the granular cells and the spinous cells and the basal keratinocytes. The largely avascular epidermis transitions into the vascularized papillary dermis at the dermal epidermal

junction. Finger like protrusions called dermal papillae comprise the papillary dermis, which is the top layer of the dermis. The reticular dermis contains other larger skin appendages such as hair follicles, sebaceous glands, eccrine glands

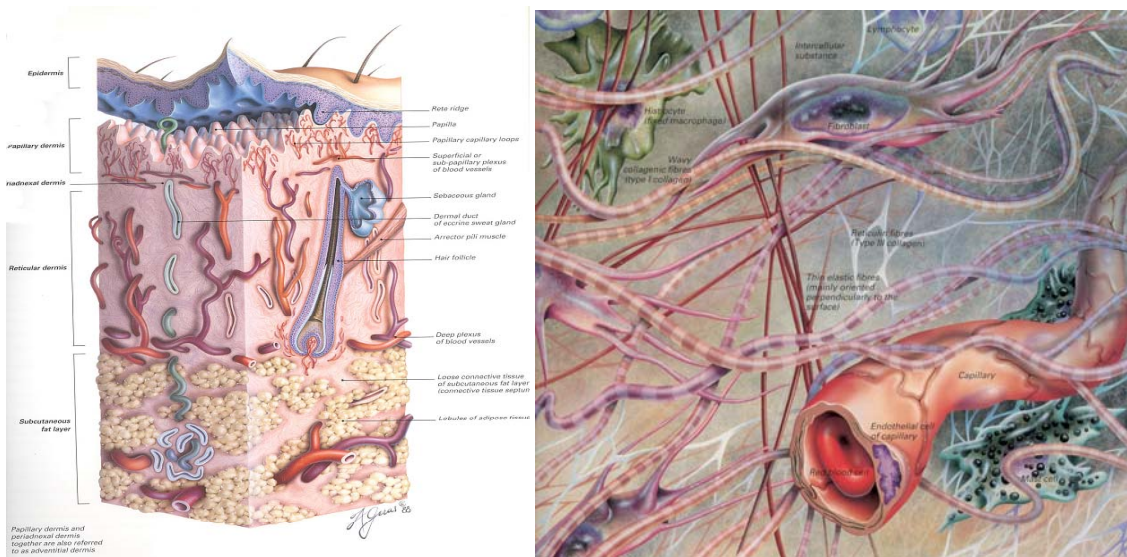


Figure 1 – (Left) Illustration of skin and its different tissue layers. The top is the epidermis, next is the reticular and papillary dermis and at the base is the subcutaneous fat. (Right) Illustration of the extra cellular matrix as well as all of the microstructure present within the papillary and reticular dermis.[4]

and different extracellular matrix structures. The extracellular matrix is described as anything that is a part of tissue that is not a cell. These wide varieties of structures, fibers and organelles have different densities that result in different optical properties and indices of refraction. These changes in density allow CSLM to function and provide valuable information as it sends in photons with

coherent laser light and records these back scattered light, recording changes in index of refraction to create optical sections as a function of depth non invasively.[6]

Optical Properties of Healthy Skin

Skin is comprised of many different structures that cause multiple scattering events with respect to photons that enter the surface and then escape back out of the skin. These multiple scattering events are wavelength dependent and also depend on the different kinds of chromophores, absorbers and scatterers present on the surface and within the tissue (Figure 2).[7] For instance, even with most of the scattering occurring at the surface of the skin (at the stratum corneum), there are also effects of scattering observed within the dermis. This is further complicated by the presence of absorbers, especially hemoglobin and melanin which are very strong absorbers as we move into the vascularized tissue.[8] If the blood is removed from the dermis and the penetration depth is measured as a function of wavelength (Figure 2) it can be seen that the near infrared wavelengths penetrate more deeply than visible wavelengths and at an order of magnitude deeper than the shorter wavelengths.

The pinhole physics that enable CSLM enable reduction of these multiple scattering events into an axially addressable single scattering event. There are however some instances where photons from different levels enter past the

Multiple scattering events and penetration depth (um) as a function of wavelength in the bloodless dermis

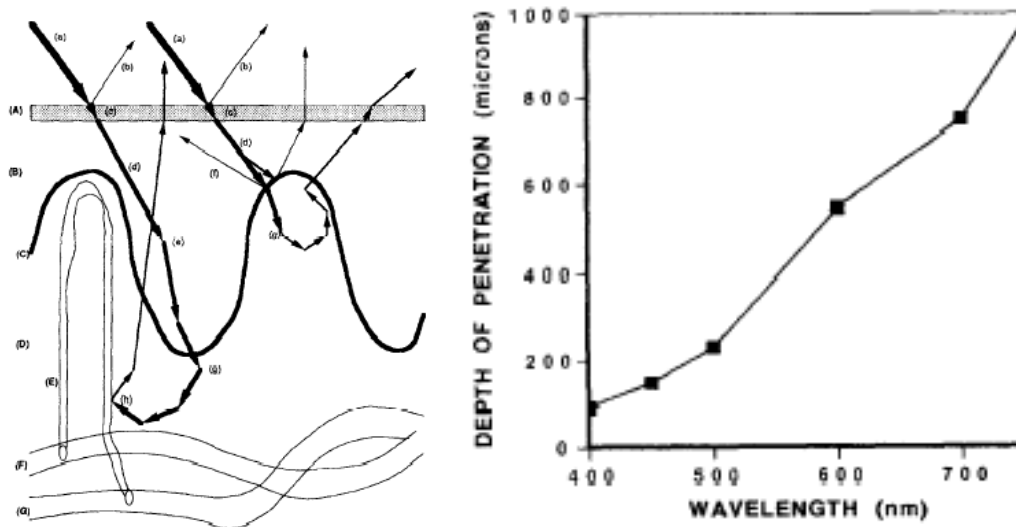


Figure 2 -- (Left) Illustration of the multiple scattering events as photons progress through the skin. (Right) Graphical representation of penetration depth (um) as a function of wavelength in bloodless dermis. Note the lower penetration at shorter wavelengths of light due to higher indexes of scattering and order of magnitude increase at longer wavelengths. These figures only consider scattering and do not consider the absorption. CSLM allows visualization of single scattering events.[7]

pinhole and will be expanded further within the coming chapter regarding

Confocal Scanning Laser Microscopy Theory.

Endogenous Skin Chromophores

Skin has many different endogenous chromophores that have unique physical characteristics. Aside from many optical scatterers found within skin, there are many absorbers and other fluorescent chromophores as well (Table 1). [7-9] In fluorescence, a particular stimulus at a given excitation wavelength elicits an emission at a higher wavelength due to the Stokes shift and basic principles of fluorescence.[10] If coherent light of a specific wavelength is used in conjunction with appropriate filters and a detector sensitive enough to measure the fluorescence signal, endogenous (and exogenous) chromophores can be measured quantitatively from the skin surface. [8]

In summary, skin is very complex with different appendages and structures that can scatter light. Not only scattering can occur in healthy skin, but also absorption and fluorescence from different chromophores located within the skin. Table 1 lists some of these endogenous chromophores found within skin.

Table 1 – Different endogenous chromophores within skin at wavelengths of interest. [7-9]

Endogenous chromophores in skin	Characteristic	Principle wavelength (nm)
Melanin	absorber and scatterer	Monotonic increase to short wavelength
Collagen crosslinks	fluorescent	X335 M380; X370 M460
Elastin crosslinks	fluorescent	X420 M500; X460 M540
Oxy Hemoglobin	absorber	412, 542, 577
Deoxy Hemoglobin	absorber	430, 555, 760

Confocal Scanning Laser Microscopy Theory

Confocal microscopy combines the fundamentals of light microscopy with the physical properties of a pinhole to achieve non-invasive optical sectioning capability.[10] The pinhole can reject multiple scattering events to generate a single point source or scattering event at an addressable point within a thick sample. When this point of light is rastered across the surface at about 10 frames per second the intensity can be recorded into an array to create an image. A basic example of this phenomenon is illustrated by comparing

conventional widefield light microscopy and the point source of confocal microscopy (Figure 3).

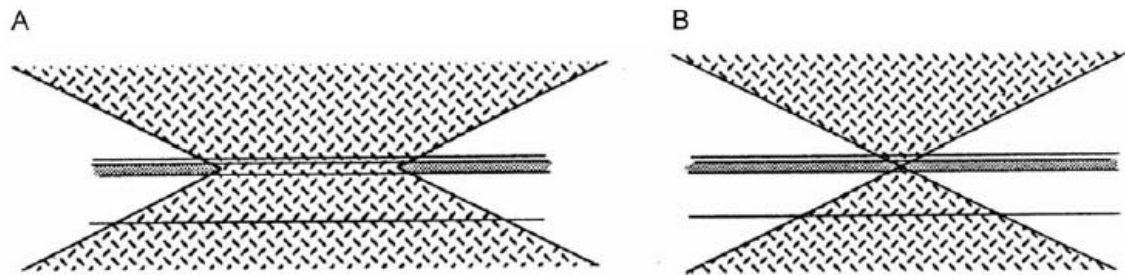


Figure 3 – Illustration of amount of incident photons with wide field and point source illumination. On the left the wide amount of light and photons that are allowed to be viewed in wide field conventional light microscope (A) and are illustrated on the right (B) the point source principle of the confocal microscopy is illustrated.[11]

To further examine the point source phenomenon it is useful to compare objects in a turbid thick sample at different depths by illustrating what would happen with conventional wide field microscopy with different target objects at different focal depths (Figure 4 (Items 1 and 2)). [11] Incoherent light used with just a pinhole is displayed in Figure 4 (Item 2). To further illustrate what occurs within CSLM, a single point source is used along with a pinhole (Figure 4 (item 3)). Undesired photons can be rejected from other structures with the presence of a pinhole, and even more so with just a focused point source which helps reduce the extra photons. As ideal as this may seem, even coherent light sources that are

focused to a single point do have mild contributions from the upper and lower layers as a second order effect.[12] The immersion media chosen and endogenous chromophores that contribute to the overall signal and intensity registered at the detector and are classified as contrast agents.[13] These facts are critical to this thesis and will be discussed in further detail in the discussion section.

In Figure 4 part 3, along the path of this point source there are photons that pass through different media that have different indexes of refraction that change the intensity of the photon by means of shifting its direction.[6] The bending of light as it enters the skin depends on how many changes in refractive index are occurring due to changes in the path of the original photons corresponding to the changes in index of refraction. This is modeled in Figure 5.

Imagine a point source that is now rastered across a controlled field of view. The single scattering events are then fed into a detector that measures intensity and places these intensities into an array of pixels that create a mosaic

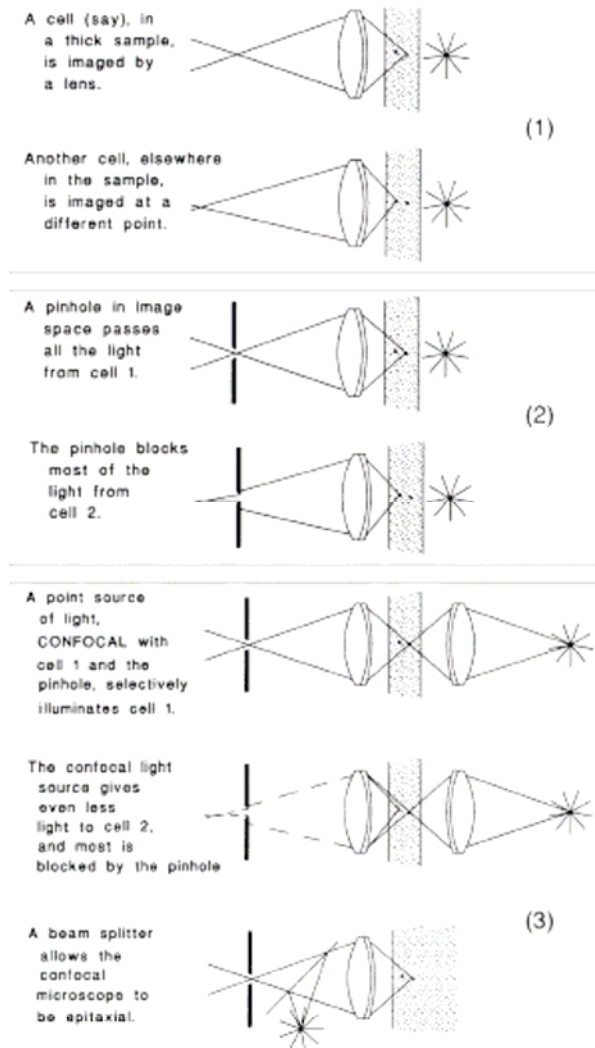
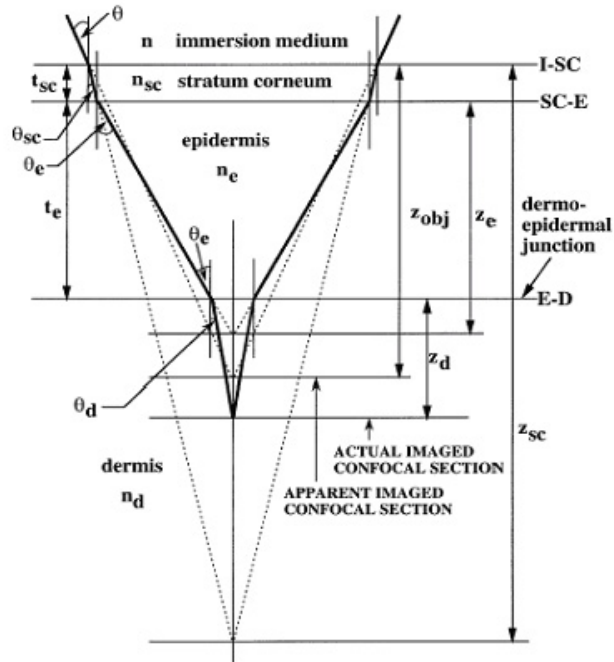


Figure 4 – Figure of confocal light properties, as they are observed through a conventional light microscope (1), using a pinhole with the conventional microscope (2) and using a pinhole and point source illumination (3). Figure and captions extracted directly from cited source.[11]

resembling an image of this optical section. These grayscale intensity values are at an 8-bit resolution, range from 0 to 255 and represent a single scattering event both at that given axial depth, and laterally within the field of view.



The immersion medium (water) and the three layers (stratum corneum, epidermis, dermis) of the skin are modeled as plane parallel layers with uniform refractive indices. The measured refractive indices are $n = 1.33$ (water), $n_{sc} = 1.51$ (stratum corneum), $n_e = 1.34$ (epidermis), and $n_d = 1.40$ (dermis). The measured thickness are $t_{sc} = 20 \mu\text{m}$ (stratum corneum) and $t_e = 100 \mu\text{m}$ (epidermis). Refraction occurs at the interfaces between the immersion medium and stratum corneum (I-SC), the stratum corneum and epidermis (SC-E), and the epidermis and dermis (E-D). The angle of incidence is θ , and the angles of refraction are θ_{sc} , θ_e , and θ_d . The depth through which the objective lens has been translated (i.e., apparent depth below the I-SC interface) is z_{obj} , for which the actual depth of the imaged confocal section is $(t_{sc} + t_e + z_d)$, calculated from equation (C.4) to (C.6).

Figure 5 – The above model represents changes in index of refraction and the subsequent bending of a ray of light as it enters the skin. Figure 5 fully extracted from source. [6].

The measured light intensity depends on how the index changes relative to the surrounding tissue.

Axial Resolution, Lateral Resolution and Point Spread Function

In summary, the basic elements of CSLM involve a coherent laser incident point source, optics and a pinhole to filter out unwanted photons to generate a thin optical section within a thick turbid sample with one resel passing through the pinhole. Resels are representative of the smallest resolvable spot generating the smallest possible focal point in confocal imaging. This thin optical section is characterized theoretically by the axial (Eq1) and lateral (Eq2) resolution equations:[6]

$$\Delta z = \frac{0.95n\lambda}{NA^2} \quad (\text{Eq1})$$

Where 0.95 is the constant used for a point source measurement (1.4 is used for a line source), n is the index of refraction of the immersion media, λ is the emitted light wavelength and NA is the numerical aperture of the objective being used. The lateral resolution is measured by the following (Eq2):

$$\Delta x = \frac{0.46\lambda}{NA} \quad (\text{Eq2})$$

Where λ is the emitted light wavelength, and NA is the numerical aperture of the objective being used. These equations when solved with the theoretical values are far better than what is achieved in reality due to the associated loss of photons and the physics of the pinhole and resolvable points required for *in vivo*

confocal microscopy. By characterizing the point-spread function of a particular microscope setup one can measure the actual axial and lateral resolution of the CSLM (Figure 6).

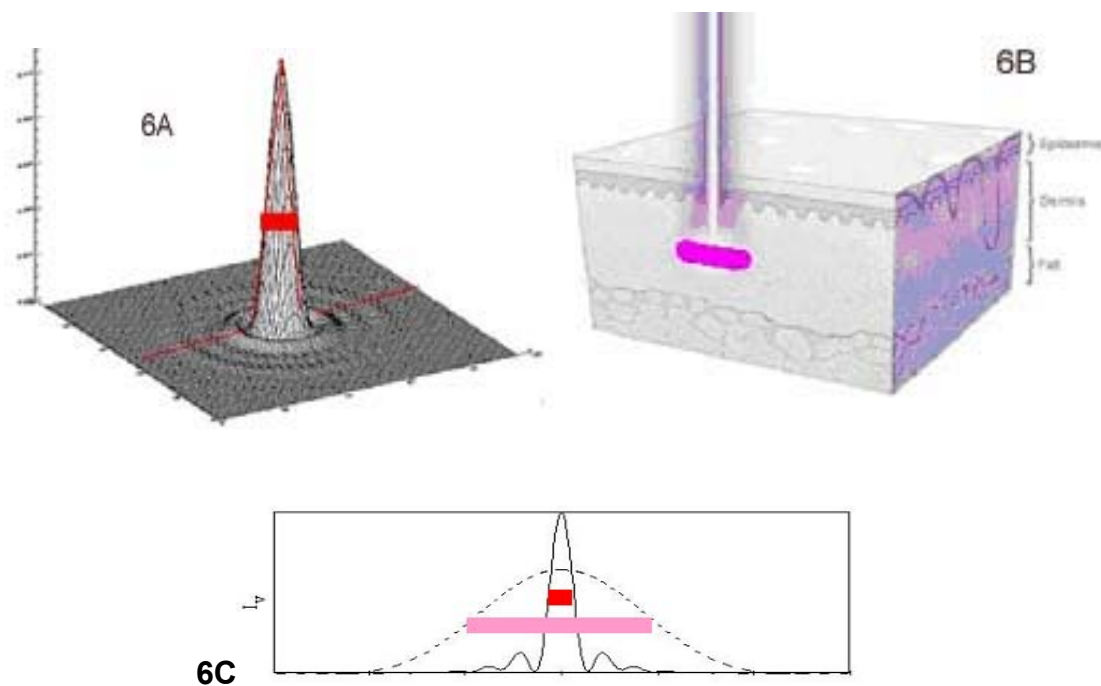


Figure 6 – 6A is a 3D example of a single theoretical resel. The thin red line in 6A is the 2D representation of a cross-section in a the narrow Gaussian distribution in 6C. The full width at half maximum of the measured intensity is the theoretical optical section. 6B is a simple skin illustration of a coherent laser point source in it to illustrate what typically happens to a point source illuminating the skin. Note pink bar and the subsequent cross section in 6C. 6C is a 2D representation of the cross section represented in red and pink for the theoretical and measured points spread functions respectively. 6A, 6B, 6C were compiled and edited and were fully extracted from the following cited websites [14-16].

The point spread function (PSF) describes the response of an imaging system to a point source or point object. The PSF is determined by many factors relating to the optics of a particular SCLM design. One of the most important features in the microscope design is the objective and the numerical aperture of the lens used.[10] The objective has most of the impact on the confocal nature of the microscope more so than the pinhole. However, if the pinhole is too large, then it is as if the pinhole is not there and the optical section is infinitely thick. If the pinhole is too small, then not enough light can pass through the pinhole. The associative effects of changing the pinhole and its effects on PSF are best illustrated in Figure 7. Imagine the full width at half maximum height and how it depends on pinhole size. The smaller the pinhole, the smaller the axial resolution.

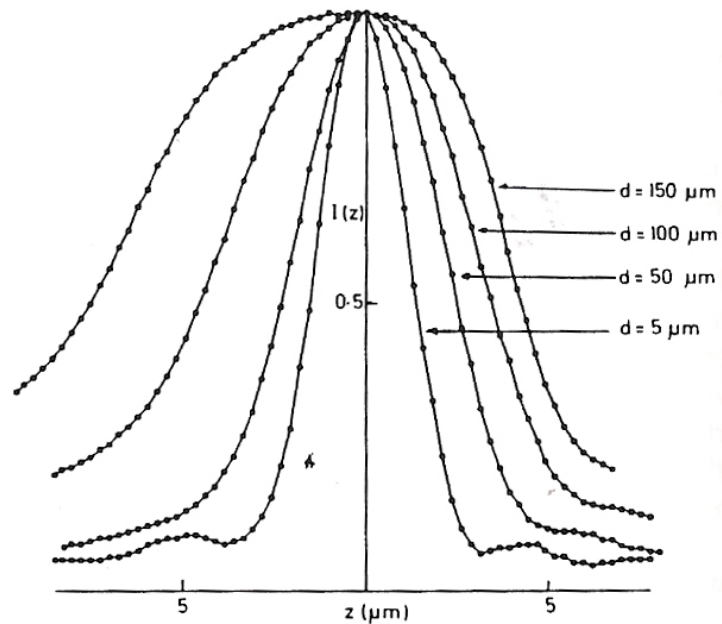


Figure 7 – Effect of pinhole size “d” in microns on point spread function (PSF). Note as pinhole widens (d increases), the subsequent PSF is broader and the FWHM also increases. This illustrates that the focal volume increases in size as the pinhole size increases.

The *in vivo* CSLM used in this experiment typically has a 3 resel pinhole relative to the wavelength. This generates enough light passing through the microscope to allow the good signal to noise ratio that is necessary for smooth skin representation by *in vivo* CSLM images. According to the manufacturer, if the *in vivo* CSLM pinholes are limited to just one resel the images appear to be grainy, even though the measurement achieved with the scope would appear to be ideal.

The microscope's actual axial resolution is generally assumed to be determined by measuring the point spread function and determining the full width at half maximum. Once these parameters are characterized for a given system the optics can be assumed equivalent so that comparisons can be made across instruments even if different incident laser wavelengths are used.

Factors Affecting SCLM

There are two main contributors to variation when using SCLM to measure human skin *in vivo*. The first is due to the optics in the microscope and the second is due to the human skin tissue. Each one of these equally shares a degree of complexity, and both are challenging to keep constant to make observations with select experimental changes. In this thesis we attempted to hold some of these variables constant in order to make assumptions about what is observed and be able to make comparisons.

It is very difficult to model optical measurements through turbid media and generate predictable images from these optical sections. Human skin is incredibly complex in structure and function and scatters light readily in different ways depending on which depth and skin layer the light is at. Optical skin phantoms are created to simulate the basic scattering and absorbing properties of structures found within skin. Developing a phantom (*in vitro* model) that can

be a close representation of skin as possible is challenging and is sometimes pursued as the subject of an entire thesis on its own.[17, 18] Certain assumptions and choices have to be made within these models in order to simulate desired scattering and absorption as found within real skin.

With further regard to modeling, mathematical models and Monte Carlo simulations can be used to estimate the path of individual photons as they enter skin and are scattered through multiple scattering events before they diffuse and exit the skin.[18, 19] The uniqueness of confocal microscopy is that it allows measuring the intensity of and visualization of single scattering events within the skin at a particular depth with minimal contributions from the different layers. A few of the optical variations are aberrations and will be covered in the next section.

Optical Variability

Aberrations

There are principally five main aberrations that can occur within monochromatic optics: spherical, coma, astigmatism, flatness of field and distortion. All of the above are within a particular wavelength of light, but there are additional aberrations present and important to discuss: the chromatic aberrations, the longitudinal chromatic aberration and lateral chromatic aberrations.[10]

With all of these factors that challenge proper CSLM functionality, the need to fix or reduce these variables to be within tolerances to allow comparisons across microscopes becomes apparent. Detailed microscope design and subsequent design of all its optical components are out of the scope of this particular thesis. However, the fact that these aberrations do exist creates issues for the proper visualization of skin and needs to be accounted for in the discussion because these factors may contribute to the observed results.

Immersion Media

Immersion media are key to obtaining clear consistent images with CSLM. There are two locations where the immersion media are placed, above and below the coverslip. For the purposes of this thesis, it is assumed that if a given objective requires either water or oil to function it is above the coverslip and cannot change because of the optical path design. The immersion media important for discussion are those below the coverslip- or what comes in contact with the skin surface or the optical skin phantom.

Different immersion media have intrinsic values that allow them to either optically match or contrast with the index of refraction and the desired skin structure (Table 2). If there is a large difference in index of refraction a large change in intensity is measured within a confocal microscope image. If there is an index of

refraction match, then the sample becomes optically transparent. A change in immersion media is a means to either provide contrast or transparency to visualize skin structure better.

Table 2 – Immersion media, their indices of refraction and skin features best imaged with these substrates.

Substrate	Index of Refraction	Skin Characteristic Visualized
Air	1	High contrast surface imaging
Water	1.33	Stratum Corneum surface imaging
Oil (Crodamol CGS)	1.50	Dermis
Oil Gel (Cargile CK)	1.54	Dermis

Hypothesis

There should be little or no change observed in reflectance mode when an 830nm CSLM is outfitted with a 785nm laser due to the close proximity in wavelength. This should result in equivalent performance with added fluorescent probe functionality.

There should be measurable changes in resolution between a 405nm and an 830nm CSLM with the added benefit of fluorescent capabilities.

There are two major forms of variability that can be experienced throughout *in vivo* CLSM imaging, skin variability and the optics of the microscope. If some of these variables are kept constant, experimental changes to the wavelength system should be able to be observed and measured.

Description of Experimental Procedure

Three main experiments were performed to highlight differences observed among the different wavelengths. They were:

- Microscope characterization
- Optical skin phantom imaging across the different wavelengths
- Human study (n=8) using the microscopes

Microscope Characterization

The confocal microscopes used in this thesis are all based upon the commercially available Vivascope 1500. The CSLMs were developed by Lucid Inc. (Rochester, NY) and were developed on commission. The stock Vivascope 1500 was on loan from the company throughout the experiments to aid with the measurements (Figure 8). The three investigated wavelengths used in the microscopes were 405nm, 785nm and 830nm.

The 830nm wavelength is the current industry standard wavelength used in reflectance mode for commercial *in vivo* CSLM units today. The two experimental wavelengths are the 785nm and 405nm.

The 785nm wavelength was chosen for its close proximity to the 830nm in the near infrared to increase penetration into the skin as well as its ability to visualize

the exogenously applied fluorescent probe indocyanine green (ICG) that has an excitation wavelength of 785nm and emission wavelength close to 814nm.

The 405nm wavelength was chosen to image in reflectance mode with higher resolution due to the smaller wavelength and to allow for visualization of endogenous fluorophores as well as exogenous fluorescent probes placed on the surface of the skin.



Figure 8 – Image of the commercially available scanning laser confocal microscope the Lucid Vivascope 1500. Current standard wavelength is 830nm and experimental wavelengths used were 785nm and 405nm for their ability to do both reflectance mode imaging in addition to fluorescence mode imaging. Note, these are fluid immersion objectives and both oil and water objectives were used to see if there was a significant difference in resolution between the microscopes. NOTE example of tissue ring and coverslip mechanism that attaches microscope to human skin is a part of the optical design and optical path of the microscope (Images courtesy of Lucid Inc.).

Special care was taken to use similar optics across all instruments. The 785nm and 830nm CSLM had the same optics, anti reflection coatings and objectives. For all measurements throughout this thesis, the same objectives were removed and used for both microscopes. The 785nm and 830nm microscopes use a 100um pinhole while the 405nm has a 50um pinhole to allow for comparable optical sectioning and smooth skin measurement within the images. The telescope optics are similar across the microscopes and generally have parity, except that the 405nm microscope has a broader spectrum telescope design and coatings that allow for less chromatic shift, important for broad spectrum fluorescence imaging. The coating on the polygon mirror facets of the 405 microscope was different as well (Enhanced Aluminum 04 instead of gold) to allow more efficient light reflection. Also, the objective was designed to be as broad spectrum as possible to remove any chromatic aberrations. An additional important difference is that a photomultiplier was used instead of a photodiode in the 405 microscope as well.

These relative changes and adjustments were necessary to allow for comparisons across the microscopes in order to maintain a relative similarity despite the large change in wavelength.

Due to the theoretical limits of the confocal technology, using a shorter wavelength in a confocal application does not seem practical for depth penetration. However, for epidermal penetration short wavelength provide

increased resolution. A 405nm coherent point source is sufficiently novel and sectioning endogenous fluorescence was believed to be impossible before this work due to the lack of penetration of the 405nm light into the skin as compared to the near IR microscopes.

Point Spread Function Measurement

The point spread function (PSF) describes the response of an imaging system to a point source or point object. The point-spread function was measured by imaging the refractive index change from immersion media with a 0.75mm acrylic coverslip that is conventionally used between the objective and the *in vivo* tissue. An image stack is acquired as a function of depth and the intensity changes with the index change from the immersion media to the top of the coverslip from dark to bright to dark again. This generates a curve with a Gaussian type shape to it. The program used to measure this takes a sub sample of the center of the confocal image and calculates the average value of the center of the image (taking a sub sample from the corners of the image). This value is then normalized by dividing the average intensity value within the image by the emitted laser power at the end of the objective (To examine the code see Appendix A – IDL code used for normalizing confocal images as a function of depth analysis). The full width at half maximum (FWHM) is then used to

represent the axial resolution and ultimately the focal volume for that particular microscope and point source.

Spatial Calibration of the Microscope

A specialized ruler was used as a standard to measure the optical field of view measured across the microscopes. The standard used is the Precision Ronchi Ruling Slides Edmund Scientific P/N M38-260. This standard allows for the direct xy spatial calibration by means of aligning the rulings in both the galvometer direction (y axis) as well as the polygon facet direction and is also the direction of the rastering of the point source (x axis) across the field of view. This allows for calibration across microscopes. Since there are lines along the ruled standard simple counting these lines and ensuring they are the same across the microscope calibrates the different microscopes. Software settings then correct for the slight differences among the different microscopes. In all our experiments we verified that differences in the field of view were negligible and all were calibrated prior to the start of the study so with regards to lateral resolution they were equivalent

Optical Skin Phantom Imaging

Simulating human tissue with a phantom allows a comparison of the microscopes with a fixed frame of reference.[17, 18] Measurement of the same substrate across microscopes in the same exact location allows for direct comparison of

intensities obtained from the model. This phantom is a simplified model of the actual tissue that will be imaged. Therefore, additional experiments need to be run in order to understand how different wavelengths when used in a CSLM affect the structures to be visualized.

Developing a skin phantom to calibrate a given experimental system is sometimes the subject of an entire thesis. Due to the limit in scope of this thesis, two previously developed optical skin phantoms were obtained from previous theses and experiments. Both used silicone as the base, and TiO₂ to simulate scattering within the tissue. The main differences between the two phantoms are the absorbing chromophores that were chosen. In one phantom, carbon black was used as an absorber, and it actually increases both the amount of scattering and absorption. India ink was used in the other phantom as an absorber, it actually absorbs more than carbon black and tends to provide a response similar to skin as observed with *in vivo* CSLM.

Human Measurement Study with Different Immersion Media

A clinical proof of concept study was conducted at Johnson & Johnson Consumer and Personal Products Worldwide, Skillman, NJ. In the study center, 8 subjects were recruited and consented (Appendix C -- Subject informed consent required for J&J CPPW clinical study.) to participate in a randomized CSLM clinical study.

The 8 subjects were imaged with the three microscopes configured and characterized as above in the same upper inner arm test sites. The same wavelengths and immersion media that were used to measure the phantoms were used in the human study to evaluate the differences that appear in human skin *in situ*.

A tissue ring and coverslip was placed on the surface of the skin and the three different microscopes were used on the same exact tissue ring. Macro images were used to capture the exact location of markers on the surface of the skin to find 3 replicate stacks per wavelength for a total of 9 image stacks per arm and test site with the immersion fluid. The arm of volunteer imaged, the immersion fluid chosen and the order in which the microscopes were used were randomized to reduce the impact experimentation could have on the results. The subjects were brought in for a time span of 3 hours, 1.5 hours for each arm. Within that time period both volar upper inner arms were measured with an oil immersion objective and a water immersion objective on all 3 microscopes. The oil objective provided better imaging results and these data were primarily used throughout the study.

The same location was examined at almost micron level reproducibility across the different subjects in an attempt to minimize the tissue variability within subjects and examine wavelength changes independently.

After acquiring a color image macro and a reflectance confocal macro view to locate fiducial marks, a 0.5mmx0.5mm data stack was taken from the surface of the skin through to the upper dermis layers. This was then repeated for the other 2 microscopes and then for the other arm. Each microscope took a period of 30 minutes (or longer) per test site to find the same exact location and then acquire the data.

Results

Below are the experimental results from all three of the experiments:

- Microscope characterization
- Optical skin phantom imaging across the different wavelengths
- Human study (n=8) using the microscopes

Microscope Characterization and Modeling

Results from measuring the actual point spread function of the microscope and the subsequent theoretical differences between the microscopes are presented

in Table 3. Figure 9 demonstrates the measured FWHM axial resolution derived from the point spread function of the 785nm and 405nm microscopes on the same chart.

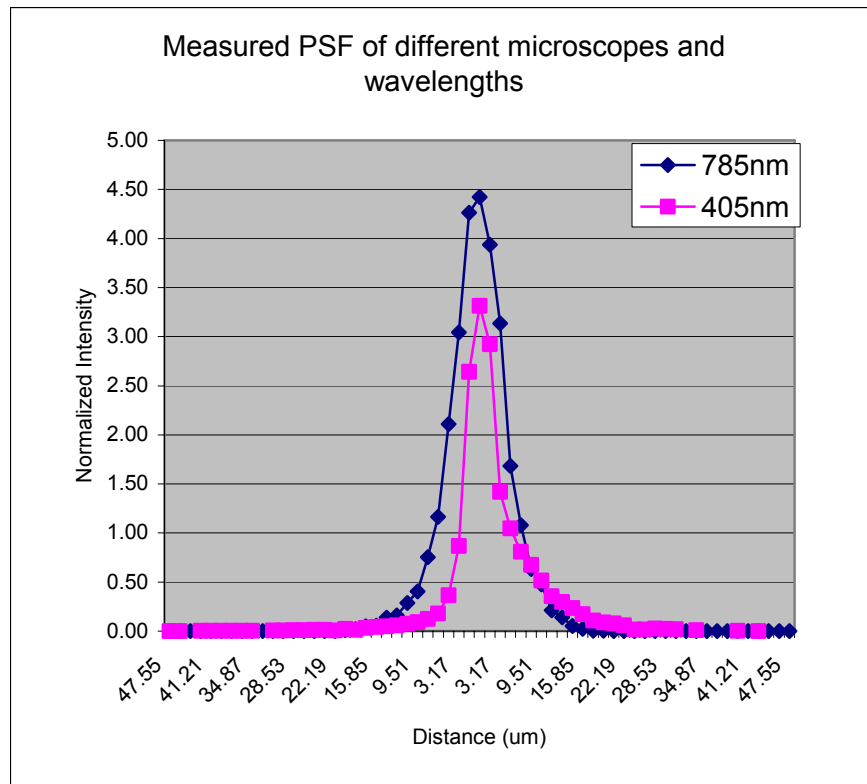


Figure 9 – Point Spread Function characterization of the microscopes. Only 785nm and 404nm are displayed on this chart to highlight the size differences in the FWHM of the PSF.

The theoretical values regarding axial and lateral microscope resolution characterizing the microscope focal volumes and the measured optical section that is the FWHM value is captured and presented in Table 3. Note- the lateral

resolution does not have a measured value, only a theoretical value because each of the microscopes are calibrated to a fixed value of 500umx500um across and adjusted within the software of the microscope to account for variability. The theoretical lateral values are what is expected for 1 resel through the pinhole and are a theoretical maximum for resolution. The focal volume is a football shape with the long axis being the axial resolution and the thickness of the shape is the lateral resolution.

Table 3 – Table of calculated theoretical axial resolution and theoretical lateral resolution (from Eq1 and Eq2 respectively) as well as the measured FWHM from the different wavelength microscopes, indicating optical section thickness. Also note- the pinhole size allows for 3 resels in *in vivo* CSLM. This is evident in the actual measured FWHM values. The actual lateral resolution is spatially calibrated across units so is not accounted for with an actual measurement.

Wavelength (nm)	Theoretical Axial Resolution (um)	Theoretical Lateral Resolution (um)	Measured FWHM (um)	Pinhole Size (um)
830	1.46	0.424	7.93	100um
785	1.38	0.401	7.93	100um
405	0.71	0.207	4.75	50um

Phantom Measurement with Different Laser Wavelengths

An optical tissue phantom was then used across all microscopes to allow wavelength comparisons on a similar frame of reference with oil immersion

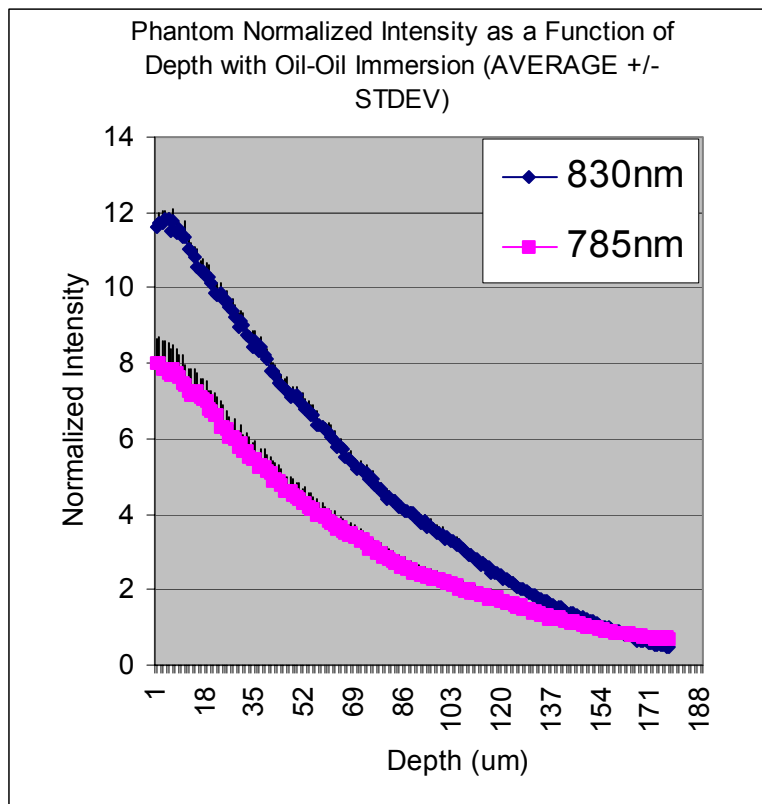


Figure 10 – Data presented using 6 replicate stacks on the optical skin phantom with oil immersion. Note- the data are highly reproducible and there is a significant increase (40% at the maximum value) of the 830nm data compared to the 785nm data.

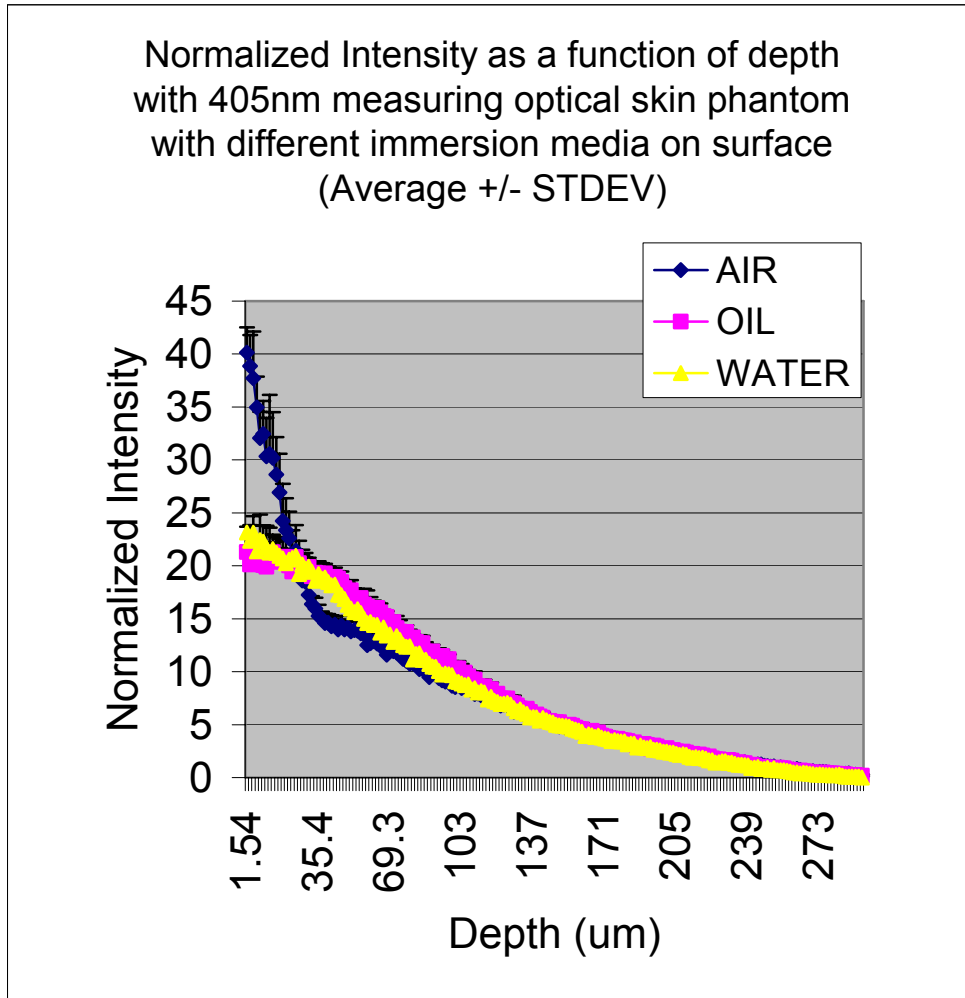


Figure 11 – This figure compares measurements of the same optical skin phantom in the same location with the 405 microscope and different immersion media. No direct comparison was made among all wavelengths because different objectives were used as well as different coatings. Note that intensity in air is higher than in oil or water. Note that the surface intensity of the water is higher, but the subsurface signal intensity on the oil measurements increases as a function of depth.

media. This allows subtle differences due to wavelength to be highlighted. The 405nm response of the phantom is illustrated individually because of the different coatings and optics used for the experimentation.

Human Skin Study: Measurements at Three Wavelengths

This experiment was to test human skin with the different wavelengths and characterize its response. There were differences observed in the intensity as a function of depth. All of the data were analyzed with the IDL code (Appendix A). However, due to specificity of skin structures select examples were reanalyzed with the Appendix B code to provide even more accurate results as presented in Figure 12-Figure 14. Appendix A and Appendix B (the two different programs) differ in how the area of interest is selected and analyzed across all of the image stacks. In theory the average intensity of the 8 bit images is normalized by the power output as measured at the end of the objective.

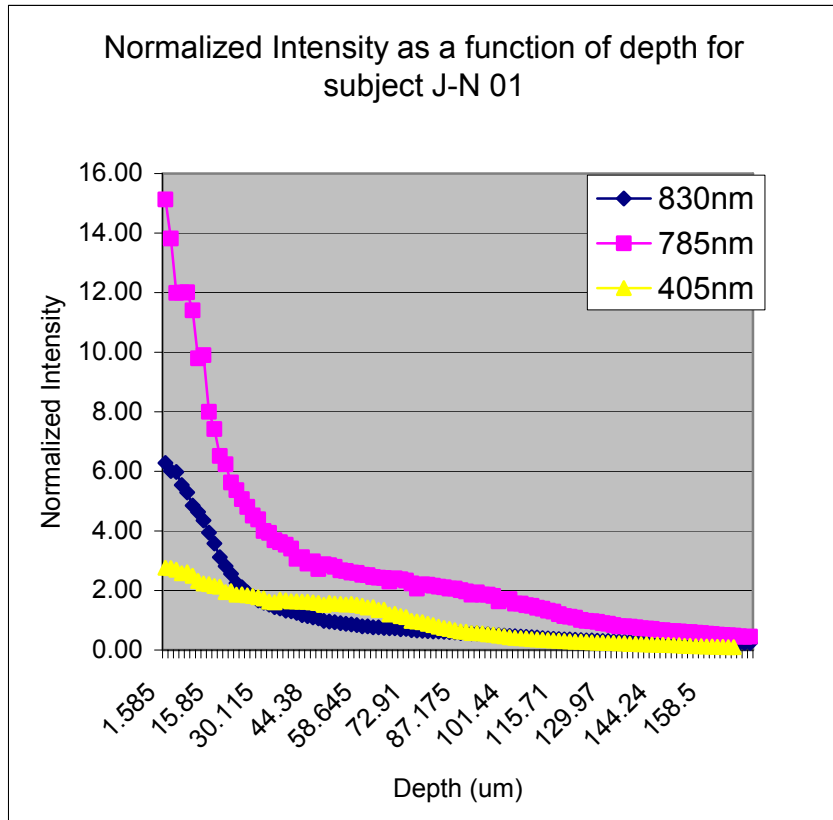


Figure 12 – Normalized intensity as a function of depth for subject J-N stack 01 (Images in Appendix D). These data are representative of the apparent change in normalized intensity of the confocal image signal as a function of depth. Note there is a higher overall measured signal with the 785nm confocal images. Also note there is an intensity increase with the 405nm around a depth of 45um, corresponding to the DE junction. This is due to the papillary collagen measured within the dermal papillae.

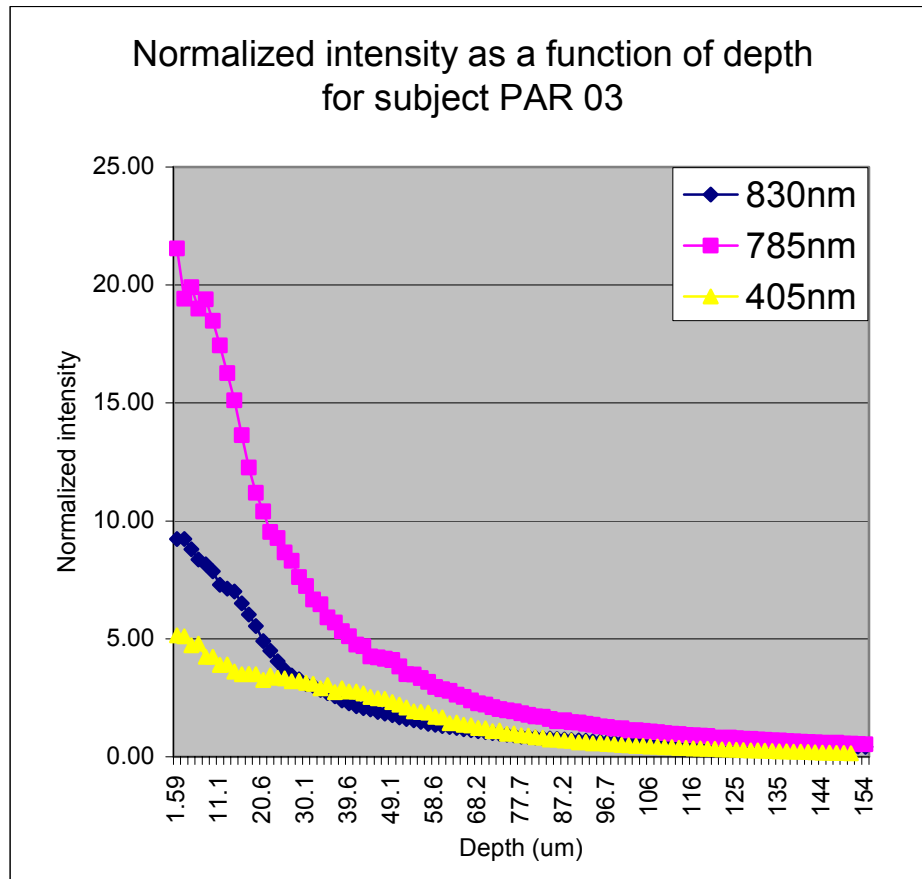


Figure 13 -- Normalized intensity as a function of depth for subject PAR stack 03. These data are representative of the apparent change in normalized intensity of the confocal image signal as a function of depth. Also note there is an intensity increase with the 405nm around a depth of 45um, corresponding to the DE junction. This is due to the papillary collagen measured within the dermal papillae.

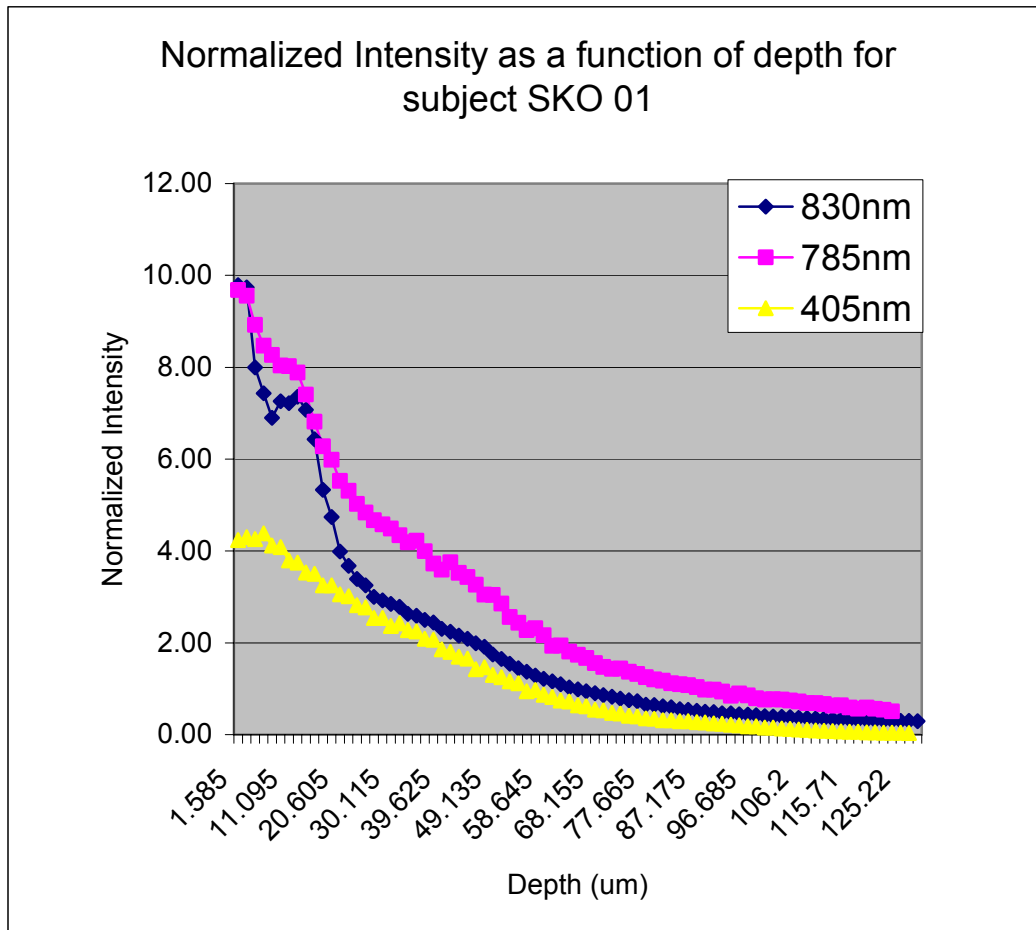


Figure 14 -- Normalized intensity as a function of depth for subject SKO stack 01. These data are representative of the apparent change in normalized intensity of the confocal image signal as a function of depth. Note there is a monotonic decrease in the 405nm signal around 45um, at the DE junction. This is due to the presence of melanin measured within the dermal papillae at the 830 and 785 wavelengths.

Discussion

The discussion below is organized based upon the three main experiments that were performed:

- Microscope characterization
- Optical skin phantom imaging across the different wavelengths with oil immersion
- Human study (n=8) using different wavelengths

Microscope Characterization

There are many factors that effect the microscope characterization. Using similar objective magnification, coatings and optics across all the microscopes was an attempt to minimize variability due to the optics of each system. Comparable design accommodations were made to allow for correction of the wavelength (decreasing by half as experienced with the 405nm wavelength, vs. the 785/830nm wavelengths).

Pinhole Size

When a smaller pinhole is used in the 405nm microscope, the images are more resolved compared to the longer wavelengths. If a comparison is made between an image of an optimized 405nm microscope with a 35um pinhole and a standard 830nm microscope with a 100um pinhole (Figure 15), one can clearly

see that there is an improvement in the overall imaging achieved with the 405 microscope. This increase in resolution is important to studying morphology and the other epidermal structures without exogenously applied contrast agents.

What is also important besides noticing the increase in resolution is the wide range of skin layers that are imaged within a given optical section. The 830nm microscope generates images that have a large optical section and vary with the different epidermal skin layers that are visible within the same section. The 405nm optical section is smaller, but the same variability across an optical section can be observed. In the lower right portion of the 405nm image you can notice the SC visualization and the granular layer becomes clearer and more regularly gridded. As you move towards the lower right side of the 405nm image, you can notice the irregularly shaped cells that are the corneocytes as they flatten and begin to comprise the stratum corneum.

Optics

Optics contribute to probably the largest variability across the different microscopes. If optics are held constant, then if wavelength is the only variable one can assign observed changes to only wavelength variation. The exact same objective, antireflective coatings and telescope optics were used across the 785nm and 830nm microscopes. A comparable objective, broad-spectrum

antireflective coatings and broad-spectrum telescope optics were used in the 405nm microscope.

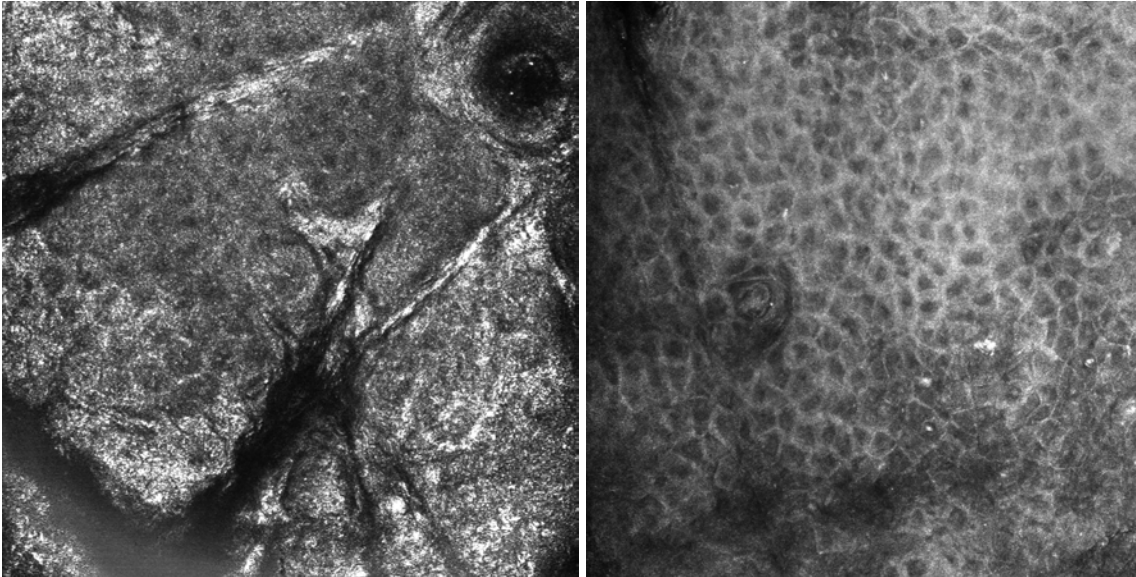


Figure 15 – On left, a 830nm CSLM image with 100um pinhole. On right, a 405nm CSLM image with a 35um pinhole. Notice the sharper delineation of the cells in the 405 image. Both images illustrate the topographical variations within one optical section. There is more variability in depth between the 830nm than there is within the 405 due to the larger optical section.

Scattering

It is challenging to discern focal volume size and identify the point where multiple scattering events begin to affect single scattering events measured by CSLM. If a larger focal volume is used then there is higher potential for the different photons to be included in this larger focal volume. These additional

photons from outside the focal volume can contribute to an increase in contrast.

[20]

Optical Phantom Experiments

The optical phantom experiments allow for wavelength comparisons across the different microscopes by means of using the fixed optical variables obtained in microscope characterization and design. Now that the optics and the phantom are held constant it is assumed that the differences in wavelength can be isolated and examined.

The CSLM intensity curves obtained from the India ink phantom resembled those obtained from skin more closely than the carbon black phantom. Once this phantom was chosen a hole was made with a piece of metal in order to establish a fixed location on the phantom. This characteristic tear was used to find the same location on the phantom and it is safe to say that this was the same exact spot on the phantom that was measured by all of the different microscopes. Six replicate stacks were then taken of the same region and averaged together to allow for statistical comparisons of the frequency response. Imaging the same phantom in the same location allows for direct comparison of the same location

within the phantom regardless of inconsistencies and inhomogeneities that may occur during fabrication of the phantom. With this amazing reproducibility and collocation of data across microscopes, changes due to wavelengths can be addressed.

In Figure 10 the 830nm and 785nm wavelengths were examined on the same microscope optics with different lasers. A 33% increase in the normalized signal as a function of depth was observed with the 830nm wavelength despite the laser power essentially remaining the same across the two wavelengths.

In Figure 11 different immersion media were compared on the same exact phantom in the same location as above in Figure 10 but with the 405nm laser wavelength. The air causes discontinuities in the optical path design and therefore causes an increase in the observed scattering towards the surface due to the large index mismatch. As oil is used, the surface of the silicone tissue optical phantom is matched allowing more scattering at depth compared to the water immersion media. This concurs with our observations *in situ* in the human imaging studies.

Note that all of 6 replicates were averaged and standard deviation was expressed in Figure 10 and Figure 11. These data are highly reproducible and demonstrate that the identical location can be imaged within the phantom

independent of the homogeneity during fabrication of the phantom. This also indicates that when the microscope is positioned in this manner only one stack, or representative record of a given location is required because of the high reproducibility of the microscope. This means that when the human study is performed, acquiring only one 500x500um image stack as a function of depth is adequate to represent the tissue in that region without taking a significant number of replicate image stacks in the same location.

Human Study Experiments

Consistent Location of Images Across Wavelengths

An important success of this thesis is the ability to reproducibly image across 3 different microscopes within the same area within a few microns *in vivo*. This is not to be trivialized as it took a long time to position the subjects, move the microscope carts, place the microscope into the tissue ring and then proceed to find the exact same 3 (500um x 500um) locations within a 4mm x 4mm image. This measurement procedure occurred within a reasonable amount of time as the subject was only available for 3 hours. Sometimes due to challenges in finding the exact same spot, it took the entire time to acquire the measurements. In summary, this technique allowed human tissue variables to be held constant so that comparisons across wavelengths could be evaluated. Making the

assumption that the microscopes are held somewhat constant and equivalent, and tissue variables are held consistent due to the co-localization of the images then comparisons regarding changes in wavelengths with *in vivo* CSLM can be investigated.

Skin Wavelength Dependent Observations

If you look at the three sample subject data images taken from different depths as in Appendix D, you can qualitatively observe the changes that occur within the human tissue due to changes according to wavelength. The main surprises are the major difference in appearance between the 785nm and the 830nm microscopes. These were supposed similar to each other, however the 785nm wavelength when compared to the 830nm wavelength as displayed in Figure 12- Figure 14 showed an increase. This may be due to absorption of the 830nm wavelength due to water present within skin.[20] Another way of expressing this larger focal volume that occurs with longer wavelengths would be to explain the contribution of the multiple scattering events as contributing to the assumed single scattering events measured by CSLM. This transition from single to multiple scattering events can be characterized mathematically by exploring diffusion theory and other Monte Carlo simulation models and is beyond the scope of this thesis.[19, 21]

The 405nm wavelength is less intense and is subject to a low penetration depth of the light and increased scattering.[7] This loss of light singly scattered back to the detector is observed as a loss of normalized intensity in Figure 12-Figure 14.

Conclusions

Proper characterization of the microscope allows for understanding of the focal volume and the lateral and axial resolution present. This has an impact on what is measured and detected with the CSLM images.

Experimental technique to locate the same identical location repeatedly has been developed and can be performed in a reasonable amount of time for *in vivo* CSLM. The 785nm & 830nm wavelengths provide essentially similar structural details but 785nm has the additive advantage of serving simultaneously as a fluorescence probe.

We have found that the 405nm wavelength allows us to better document the cellular details of the epidermis, as well as endogenous fluorescence and may serve simultaneously as a fluorescent probe

The use of a phantom allows wavelength differences to be objectively examined in a reproducible fixed frame of reference. The properties of the immersion media can be used as either contrast or index matching to allow optical transparency in a similar frame of reference.

By holding as many of the experimental variables constant as possible, comparisons across different wavelengths can occur within the CSLM images acquired.

Recommendations

It is a recommendation that a microscope be constructed with broad-spectrum telescopes and objectives that allow for simultaneous broad spectrum *in vivo* CSLM. This will allow better control of the optical variabilities of the experimental setup and reduce the complexity of attempting to fix human tissue variables to allow comparisons across wavelengths. With this frame of reference it will be possible to achieve more accurate and precise characterization of skin and enable more definitive conclusions to be generated about the observed phenomena.

Before mathematical models can be applied to measurements of biologically variable tissues, characterization and modeling of the biological phenomena should occur. Until very recent murine tissue measurement work by Steve Jacques & Dan Geareau *et al* from University of Oregon, only *ex vivo* characterization with confocal microscopy of optically thin tissue biopsies had occurred attempting to reduce biological complexity and characterize what is happening.[22] Moving into turbid media and optically thick samples leads to assumptions during characterization due to the many variables present in such applications. A reductionism model of isolating particular endogenous chromophores and studying scattering inducing structures in phantoms would be

the next steps and recommendations from this thesis. This would allow these new tools to be used in a way that provides better understanding of the phenomena in *in vivo* tissue.

References

1. Tikuisis, P., P. Meunier, and C.E. Jubenville, *Human body surface area: measurement and prediction using three dimensional body scans*. European Journal of Applied Physiology, 2001. **85**(3): p. 264-271.
2. Tagami, H., *Functional characteristics of the stratum corneum in photoaged skin in comparison with those found in intrinsic aging*. Archives of Dermatological Research, 2007. **in press**.
3. Marrakchi, S. and H.I. Maibach, *Biophysical parameters of skin: map of human face, regional, and age-related differences*. Contact Dermatitis, 2007. **57**(1): p. 28-34.
4. Geras, A.J., *Dermatology: a medical artist's interpretation* 1990, Basel: WR 100 G356 1990. 139.
5. Schoop, V.M., N. Mirancea, and N.E. Fusenig, *Epidermal Organization and Differentiation of HaCaT Keratinocytes in Organotypic Coculture with Human Dermal Fibroblasts*. 1999. **112**(3): p. 343-353.
6. Rajadhyaksha, M., et al., *In Vivo Confocal Scanning Laser Microscopy of Human Skin II: Advances in Instrumentation and Comparison With Histology*. 1999. **113**(3): p. 293.
7. Kollias, N., *The physical basis of skin color and its evaluation*. Clinics in Dermatology, 1995. **13**(4): p. 361-367.
8. Stamatias, G.N. and N. Kollias, *Blood stasis contributions to the perception of skin pigmentation*. Journal of Biomedical Optics, 2004. **9**(2): p. 315-322.
9. Doukas, A.G., et al., *Fluorescence Excitation Spectroscopy for the Measurement of Epidermal Proliferation*. Photochemistry and Photobiology, 2001. **74**(1): p. 96-102.
10. Pawley, J.B., *Handbook of biological confocal microscopy*. 2nd ed. The language of science. 1995, New York: Plenum Press. xxiii, 632 p., [4] p. of plates.
11. Webb, R.H., *Confocal optical microscopy*. Reports on Progress in Physics, 1996. **59**(3): p. 427.
12. Webb, R.H. and P.M. Conn, *[1] Theoretical basis of confocal microscopy, in Methods in Enzymology*. 1999, Academic Press. p. 3.

13. Rajadhyaksha, M., et al., *In Vivo Confocal Scanning Laser Microscopy of Human Skin: Melanin Provides Strong Contrast*. *J Investig Dermatol*, 1995. **104**(6): p. 946.
14. http://www.beckman.com/coultercounter/images/Homepage_tech_mie_3.jpg. *Image*. [cited; Available from: http://www.beckman.com/coultercounter/images/Homepage_tech_mie_3.jpg]
15. http://www.consultingroom.com/Storage/Treatment_FAQs/TDLightrejuvenation100403.jpg, *Block diagram drawing of skin with laser in it*.
16. http://www.consultingroom.com/Storage/Treatment_FAQs/TDLightrejuvenation100403.jpg, *image 2*.
17. Basu, H., E.S. Papazoglou, and Drexel University. College of Biomedical Engineering Science and Health Systems., *A novel method for calibration of a functional near infrared spectroscopy (fNIRS) instrument used in the assessment of wound healing*. 2007, Drexel University, Drexel University, 2007.: Philadelphia, Pa. p. viii, 70 Leaves.
18. Gearau, D.S. and O.H.S.U.O.S.o.S. Engineering., *In Vivo Confocal Microscopy In Turbid Media*, in *Biomedical Engineering*. 2006, Oregon Health & Science University, Oregon Health & Science University, 2006.: Portland, OR. p. 267.
19. Jacques, S., et al. *Specifying tissue optical properties using axial dependence of confocal reflectance images: confocal scanning laser microscopy and optical coherence tomography*. 2007: SPIE.
20. Dunn, A.K., et al., *Sources of contrast in confocal reflectance imaging*. *Applied Optics*, 1996. **35**(19): p. 3441.
21. Hollmann, J. and L.V. Wang. *Diffusion theory for multi-layered scattering media*. 2005. San Jose, CA, United States: International Society for Optical Engineering, Bellingham, WA 98227-0010, United States.
22. Collier, T., et al., *Determination of epithelial tissue scattering coefficient using confocal microscopy*. *IEEE Journal on Selected Topics in Quantum Electronics*, 2003. **9**(2): p. 307-313.

Appendix A – IDL code used for normalizing confocal images as a function of depth analysis

This program was a collaborative effort between Michael Luedtke, Gregory Payonk Ph.D. and Dick Jackson. It sub samples 'subrects' a full 1000x1000 pixel confocal image and then normalizes with respect to the objective laser power. This uses a square shaped region of interest that is scalable but limited to the center of the image.

====

```
PRO confocalProcess
```

```
;FILE_DELETE,'ConfocalTest2.dbf', /allow_nonExistent
```

```
!order = 1
```

```
While !D.Window NE -1 DO WDelete
```

```
UsePrecisionSelectCursor
```

```
;file naming: D:\ConfocalDataAnalysis\BPR 01-17-05\BPR 01-17-  
05\200501171751\ 01\ 01_ZMap01_Image01.BMP
```

```
.*****  
,
```

```
showProgressBar = 0
```

```
inFromEdge = 0.25 ; amount to cut away from each edge on subrecting
```

```
DBF = 'ConfocalTest1.dbf'
```

```
dbfFields = ['filename C(120)', $
```

```
    'fname C(30)', $
```

```
    'drive C(2)', $
```

```
    'dir1 C(30)', $
```

```
    'dir2 C(30)', $
```

```
    'dir3 C(30)', $
```

```
    'dir4 C(30)', $
```

```
    'dir5 C(30)', $
```

```
    'san C(3)', $
```

```
    'date C(8)', $
```

```
    'time C(4)', $
```

```
    'side C(1)', $
```

```
    'site C(2)', $
```

```
    'layer N(4)', $
```

```
    'medimg N(6)', $
```

```
    'laserPower N(7,1)', $
```

```
'xrealPos N(9)', $  
'yrealPos N(9)', $  
'zrealPos N(9)', $  
'xStep N(7,4)', $  
'yStep N(7,4)', $  
'zStep N(7,4)', $  
'depth N(9,3)', $  
'NIntensity N(9,3)']
```

```
xstep = 0.0254           ;mm
```

```
ystep = 0.0254           ;mm
```

```
zstep = 1.585            ;um
```

```
.*****  
,
```

```
IF ~FILE_TEST(dbf) THEN objDB = CreateDBF(dbf, dbfFields)
```

```
objDB = ConnectToDBF(dbf)
```

```
objRS = Obj_New('IDLdbRecordSet', objDB, Table=dbf)
```

```
dir2process = dialog_pickfile(/Directory, title='Select a Subject Directory to  
Process')
```

```
; extMatch = '*.bmp'

; imageMatch = 'image..\bmp'

; files = file_search(dir2process,extMatch, count=nFiles)

; ; the ..\ is a special syntax where a single dot means any character and the
backslash dot means an actual dot

; whImage      = Where(StRegex(files, imageMatch, /Boolean, /Fold_CASE),
Complement=whNotImage)

; allImageFiles = files[whImage]

imageMatch = '*image??.bmp'

allImageFiles = file_search(dir2process, imageMatch, Count=nAllImageFiles)

IF nAllImageFiles EQ 0 THEN Return

scrsz=get_screen_size()

IF      showProgressBar      THEN      oProgress      =
obj_new('krProgressBar',xsize=200,ysize=25,xoffset=scrSize[0]/2,
yoffset=scrSize[1]/2, /displayPercent)

nImagesDone = 0L
```

```
imageDirs = File_DirName(allImageFiles, /Mark_Directory)
```

```
imageDirs = imageDirs[Uniq(imageDirs, Sort(imageDirs))]
```

```
FOR dirI=0, N_Elements(imageDirs)-1 DO BEGIN
```

```
    imageFiles = File_Search(imageDirs[dirI]+imageMatch, Count=nImages)
```

```
    imageFiles = imageFiles[Uniq(imageFiles, Sort(imageFiles))]
```

```
    ;;thumbFiles = files[whNotImage]
```

```
    ;;*****nImages = n_elements(imagefiles)
```

```
    FOR i = 0,160 DO BEGIN
```

```
        ;;FOR i = 0,nImages-1 DO BEGIN
```

```
            print,imageFiles[i]
```

```
            img=readimage(imageFiles[i])
```

```
            WriteImage, img, JustPathNoExt(imageFiles[i])+'.jp2', /DontOverwrite
```

```
            w=imagewidth(img)
```

```
            h=imageheight(img)
```

```
            img=subimage(img,[w*inFromEdge, (1-inFromEdge)*w-1, h*inFromEdge, (1-  
inFromEdge)*h-1])
```

```
txtFile = JustDir(imageFiles[i])+JustFileNameNoExt(imageFiles[i])+'.txt'
```

```
nlines = FILE_LINES(txtFile)
```

```
parms = STRARR(nlines)
```

```
OPENR, unit, txtFile,/GET_LUN
```

```
READF, unit, parms
```

```
FREE_LUN, unit
```

```
FOR j = 0,nlines-1 DO BEGIN
```

```
  Isplit = StrSplit(parms[j], '=', /Extract)
```

```
  varName = StrTrim(Isplit[0], 2)
```

```
  assignStr = StrTrim(Isplit[1], 2)
```

```
  DJEvalExpression, assignStr, result
```

```
  (scope_varfetch(varName,/enter)) = result
```

```
END
```

```
filename = imageFiles[i]
```

```
fname = JustFileName(imageFiles[i])
```

```
filenameSplit = strsplit(imagefiles[i], '\', /extract, count=nDirs)
```

```
drive = filenameSplit[0] + '\'
```

```
dir1 = '\'+ filenameSplit[1]
```

```
dir2 = '\'+ filenameSplit[2]
```

```
dir3 = '\' + filenameSplit[3]
```

```
dir4 = '\' + filenameSplit[4]
```

```
dir5 = '\' + filenameSplit[5]
```

```
san = StrMid(filenameSplit[2],0,3)
```

```
date = strmid(filenameSplit[4],0,8)
```

```
time = strmid(filenameSplit[4],8,4)
```

```
side = STRUPCASE(strmid(filenameSplit[5],0,1))
```

```
site = strmid(filenameSplit[5],2,2)
```

```
medimg = FIX(median(img))
```

```
NIntensity = medimg/LaserPower
```

```
xRealPos = xpos
```

```
yRealPos = ypos
```

```
zRealPos = zpos
```

```
depth = 0.0
```

```
;; Layer is now simply (i+1) (index number of file in directory + 1)
```

```
layer = i+1
```



```
;; Ignore past layer calculation:
;; Sample filename: I01_ZMap01_Image01.BMP
;; Get ZMap and Image numbers from filename
;   zMapNo = StrMid(fname, /Reverse_Offset, 13, 2)
;   imageNo = StrMid(fname, /Reverse_Offset, 5, 2)
;; Calculate Stack and Layer numbers from those
;   seqNo = (Fix(zMapNo)-1)*16+Fix(imageNo)-1 ; Zero-based sequence
;   stack = (seqNo / 32)+1           ; Integer math
;   layer = (seqNo MOD 32)+1

objRS -> AddRecord,filename,fname,drive,dir1,dir2,dir3,dir4,dir5, $
       san,date,time,side,site,layer,medimg,LaserPower, $
       xRealPos,yRealPos,zRealPos,xstep,ystep,zstep,depth,Nintensity

IF           showProgressBar           THEN           oProgress-
>update,FLOAT(++nImagesDone)/nAllImages

ENDFOR ;; i over all images in one directory

ENDFOR ;; dirl over all directories
```

Obj_Destroy, objRS

Obj_Destroy, objDB

IF showProgressBar THEN Obj_Destroy, oProgress

END

;

;The motor offsets are

;X - 200

;Y - 195

;Z - 6936

;So subtract these from the absolute motor positions

;and multiple by the conversion to get your distance.

Appendix B – MATLAB code used for enhanced normalized intensity analysis as a function of depth

This MATLAB code was developed by Yang Liu Ph.D, and was used to calculate the normalized intensity of the human data more precisely to account for skin structures. This is different from Appendix A in that it has a customizable region of interest that can be any shape, not just rectangular, and can more accurately measure the normalized change in index of refraction.

====

readpower.m (reads objective laser output from text file)

```
function laserpower = readpower(file)
```

```
%addpath('E:\Data\');
```

```
%file = '01_ZMap01_Image01.txt';
```

```
fid = fopen(file);
```

```
for i = 1:3
```

```
    junk = fgetl(fid);
```

```
end
```

```
tmp = fgetl(fid);
```

```
laserpower = str2num(tmp(12:end));
```

```
fclose(fid);
```

====

read_confocalimages.m

This program calls readpower.m to get laserpower readings from text file and then performs normalization procedure with the user selectable region of interest.

```
clear all;
```

```
close all;
```

```
% specify your path
```

```
dirpath = 'F:\Local Files\working\wavelength oil and water working\confocal  
example data\PARO405\03';
```

```
%Zmap_num = ['01';'02';'03'; '04'; '05'];
```

```
Zmap_num = ['01';'02';'03'; '04'; '05'; '06'];
```

```
%Zmap_num = ['01';'02';'03'; '04'; '05'; '06'; '07'];
```

```
%Zmap_num = ['01';'02';'03'; '04'; '05'; '06';'07';'08'];
```

```
%Zmap_num = ['01';'02';'03'; '04'; '05'; '06';'07';'08';'09'];
```

```
%Zmap_num = ['01';'02';'03'; '04'; '05'; '06';'07';'08';'09';'10'];
```

```
cd(dirpath);
```

```
lesion_indx = findstr(dirpath, '\');
```

```
lesion = dirpath(lesion_indx(end) + 1:end);
```

```
% select the image to get roi

Zmap = 'ZMap03';

sel_image = [lesion, '_', Zmap, '_Image08.BMP'];

image0 = imread(sel_image);

figure(1), imagesc(image0), colormap(gray), axis image, axis off;

[BW,x0,y0] = roipoly;

% list all the files

image_num = ['01'; '02'; '03'; '04'; '05'; '06'; '07'; '08'; '09'; '10'; '11'; ...
            '12'; '13'; '14'; '15'; '16'];

num = 0;

for i = 1:length(Zmap_num)

    for j = 1:16;

        num = num + 1;

        filenames(num,:) = cellstr([lesion, '_', Zmap, Zmap_num(i,:), '_', 'Image', ...
            image_num(j,:), '.BMP']);

    end

end

for k = 1:num;
```

```
filename = char(filenamees(k,:));  
info_filename = strrep(filename,'.BMP','.txt');  
laserpower = readpower(info_filename);  
image = double(imread(filename)./laserpower);  
new_image = image.*BW;  
intensity(k,:) = mean(new_image(:));  
figure(2),imagesc(image),colormap(gray),axis image, axis off;  
hold on, plot(x0,y0,'b','linewidth',2),hold off;  
% pause(0.5);  
end  
  
save intensity_z.txt intensity -ASCII;
```

Appendix C -- Subject informed consent required for J&J CPPW clinical study.

Investigator: Michael Luedtke J&J CS194-06
Title: Scanning Laser Confocal Microscopy Wavelength and Contrast Agent Study.
Page 1 of 5

CONSENT FORM

INTRODUCTION: You are being asked to take part in a research study. Before you give your consent to be a subject, it is important that you take enough time to read and understand what your participation would involve. In preparing this consent form, it has been necessary to use some technical language. Please ask questions if there is anything you do not understand.

You will be given a signed copy of this consent form and any other necessary written information prior to the start of the study.

PURPOSE: The purpose of this research study is to measure the structures visualized with different wavelengths on the same test site with different contrast agents. Eight female subjects 25-45 years of age will need to finish the study. The study requires you to be here for one (1) visit for three hours in duration.

TEST ARTICLES: Different types of oil and water solutions will be used in this study. All oils are currently marketed products. The investigator will be using the products together with the scanning laser confocal microscopes. You will be asked to lie still for an extended period of time so that 3 different microscopes can be used on the same test site.

NOTE: You should not participate in this study if you have any known sensitivities or allergies to oils, water, or currently marketed moisturizer and cleanser ingredients.

STUDY PROCEDURES:

You are being asked to read and sign this consent form.

ONE Study Visit – 3 hours: .You will be required to lie still for 3 hours throughout the experiment. Sites will be chosen on your arms to allow imaging with 3 different microscopes on the same exact site. Water or oil solutions will be used on the different test sites.

An adhesive ring and the immersion media will be placed gently on your skin to measure the structures within your skin (200 microns deep). The brightness and color of your skin will show different structures with the different wavelengths and immersion media.

FEMALES OF CHILDBEARING POTENTIAL: You may not participate in this study if you are pregnant or nursing because they may have an impact on your skin's condition.

FORSEEABLE RISKS OR DISCOMFORTS: The therapy and procedures to be followed in this study may involve the following foreseeable risks and discomforts. You may experience slight irritation of the test site due to the occlusion of your skin for an extended period of time.

Investigator: Michael Luedtke J&J CS194-06
Title: Scanning Laser Confocal Microscopy Wavelength and Contrast Agent Study.
Page 2 of 5

Reactions are usually due to irritation, although an allergic reaction might occur. If it is determined that an allergic reaction has occurred, you can expect an allergic reaction to the material if you encounter it at a later date. Whenever possible you will be told the name of the product that caused the allergic reaction in order that you may avoid contact with it in the future.

You should report any unusual symptoms or signs you may notice during the study, even if you consider such symptoms or signs to be minor or unrelated to the study.

UNFORSEEN RISKS: There may be risks from participating in this study that are unknown.

BENEFITS: You may or may not benefit from the applications of test articles but the study results may allow a new or improved product regimen to be marketed.

ALTERNATIVE PROCEDURES/TREATMENTS: Since this study is for research purposes only, an alternative treatment would be not to participate in this study.

PERMISSION TO RELEASE PERSONAL HEALTH INFORMATION:

This section explains how personal health information collected about you for the study may be used. Your personal health information includes, but is not limited to, information that was collected for your entry into the study and information that is collected during the study. The purpose of collecting this information is to allow the sponsor, study staff and the study investigator to conduct the study, to evaluate the study procedures, and to analyze and re-analyze the study results.

You may decide not to give permission for the release of your personal health information for the study. In that case, you will not be able to participate in the study. This is because the study staff and/or the study investigator would not be able to collect the information needed to evaluate the study procedures.

The information the study staff sends to the Sponsor does not include your name, address, telephone number or social security number. Instead, the study staff will use your initials and assign a code number to the information that is sent to the Sponsor.

The study investigator may disclose your personal health information to the IRB and to the Sponsor including people who work with the Sponsor. The people who work with the Sponsor may include data monitoring committees, contract research organizations, and consultants who have contracts with the Sponsor to do the study and review the study results.

Your study records and also your entire medical record may be inspected at the study facility, by the Sponsor, and/or people who work with the Sponsor, and by regulatory authorities in the United States, such as the Food and Drug Administration (FDA), or regulatory agencies from other countries. These reviews are done to check on the quality of the study.

Investigator: Michael Luedtke J&J CS194-06
Title: Scanning Laser Confocal Microscopy Wavelength and Contrast Agent Study.
Page 3 of 5

The results of the study may be published in a medical book or journal, or presented at meetings for educational purposes. Neither your name, nor any other personal health information that specifically identifies you, will be used in those materials or presentations.

You may ask the study investigator to see and copy your personal health information related to the study. You may also ask the study investigator to correct any study related information about you that is wrong. You may have to wait until the end of the study to see your study records, so that the study can be organized properly.

This permission to share your personal health information for this study does not have an expiration date. If you no longer want to share your personal health information, you may cancel your permission at any time by writing to the study staff at the address below:

Michael Luedtke
199 Grandview Road
Mail Stop NR 110
Skillman, NJ 08558

If you cancel your permission after you have started in the study, the study staff and the study investigator will stop collecting your personal health information. Although they will stop collecting new information about you, they will need to use the information they have already collected to evaluate the study results. If you start the study and then cancel your permission, you will not be able to continue to participate in the study. This is because the study staff and/or the study investigator would not be able to collect the information needed to evaluate the study results.

The Sponsor and Investigator will make every reasonable effort to keep your personal health information private. But after the study staff or the study investigator share your personal health information from the study, federal privacy laws may not keep it private. There might be state or other federal laws that would protect the privacy of this information.

MEDICAL TREATMENT: If in the course of this study you experience illness, discomfort or injury that appears to be a result of the study the sponsor will provide you with medical care at no cost to you. Providing such medical care is not an admission of legal responsibility. If such illness, discomfort or injury does occur, ask any staff member to arrange a meeting for you with the appropriate personnel.

In certain cases of illness or injury resulting from this study, insurance benefits may be available.

WHO TO CONTACT: If you have any questions about this study or in case of an emergency, contact Michael Luedtke at 908 874 1154. In addition, if you have any questions as to your rights as a research subject, contact Christine Folsom-Kovarik at 908 874 2594.

Investigator: Michael Luedtke

J&J CS194-06

Title: Scanning Laser Confocal Microscopy Wavelength and Contrast Agent Study.

Page 4 of 5

VOLUNTARY PARTICIPATION/WITHDRAWAL: Your participation in this research study is strictly voluntary. You may refuse to participate or may discontinue participation at any time during the study without penalty or loss of benefits to which you are otherwise entitled.

If you agree to participate in this study, you are also agreeing to provide the Investigator with accurate information and to follow study instructions as given to you. If you fail to follow study instructions, your participation may be ended.

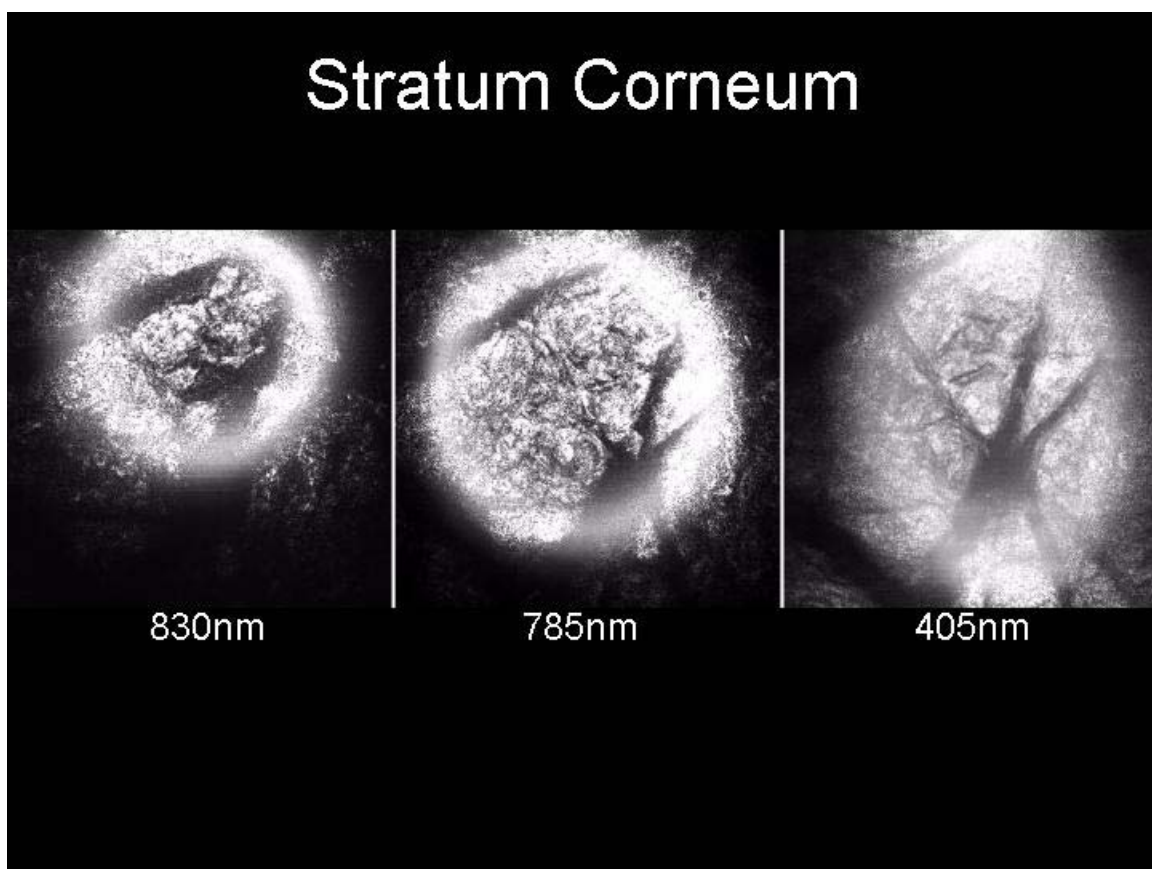
The Investigator, the FDA or the sponsoring company may discontinue your participation in the study at any time without your consent.

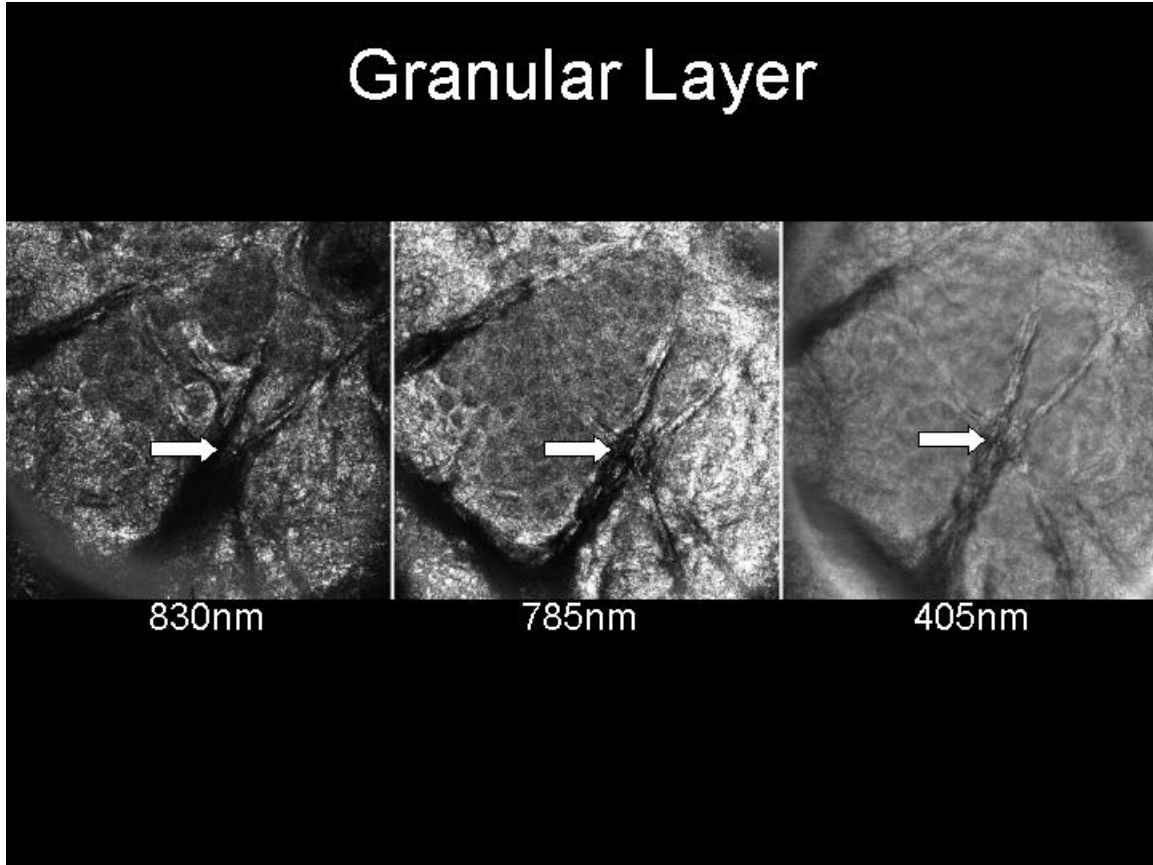
There are no anticipated expenses to you for participating in this study. All test related materials will be provided at no cost to you. They will be collected at the end of the study.

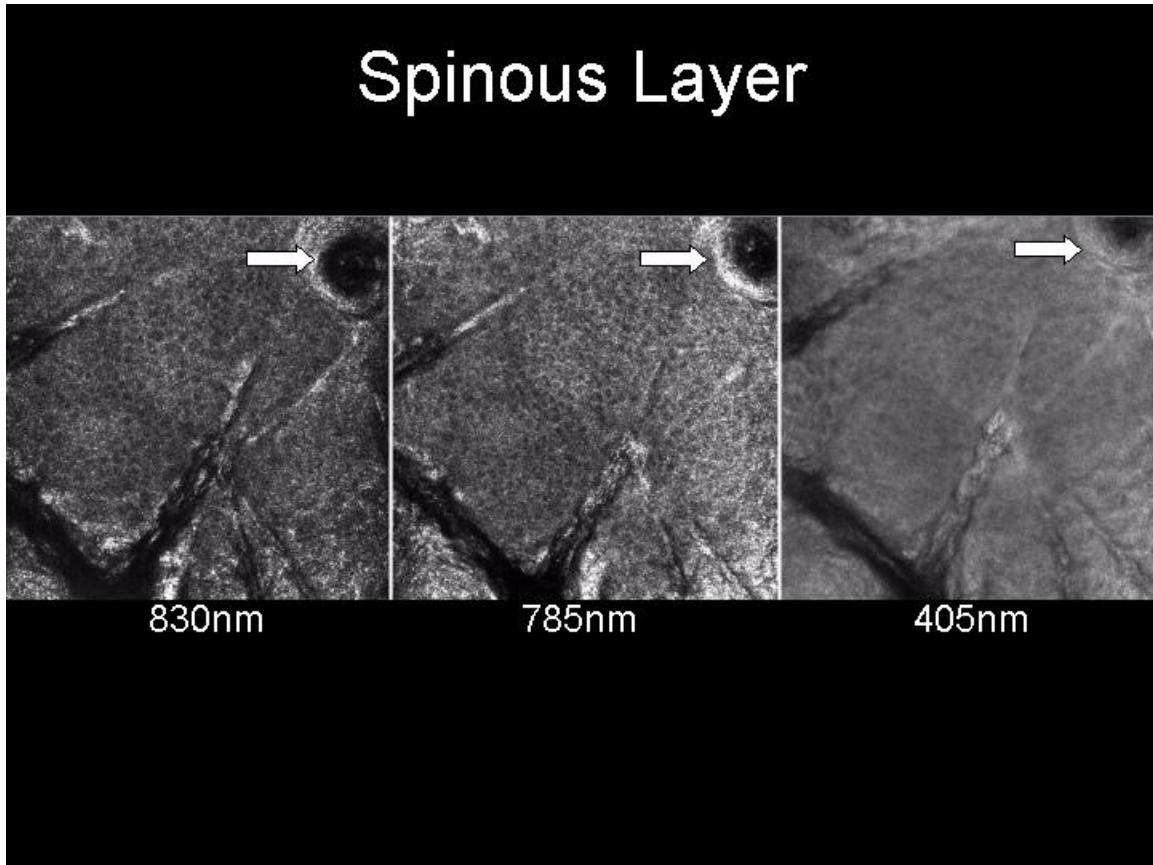
SUBJECT COMPENSATION: For your complete participation in this study you will have \$100 USD deposited to your account at no cost to you.

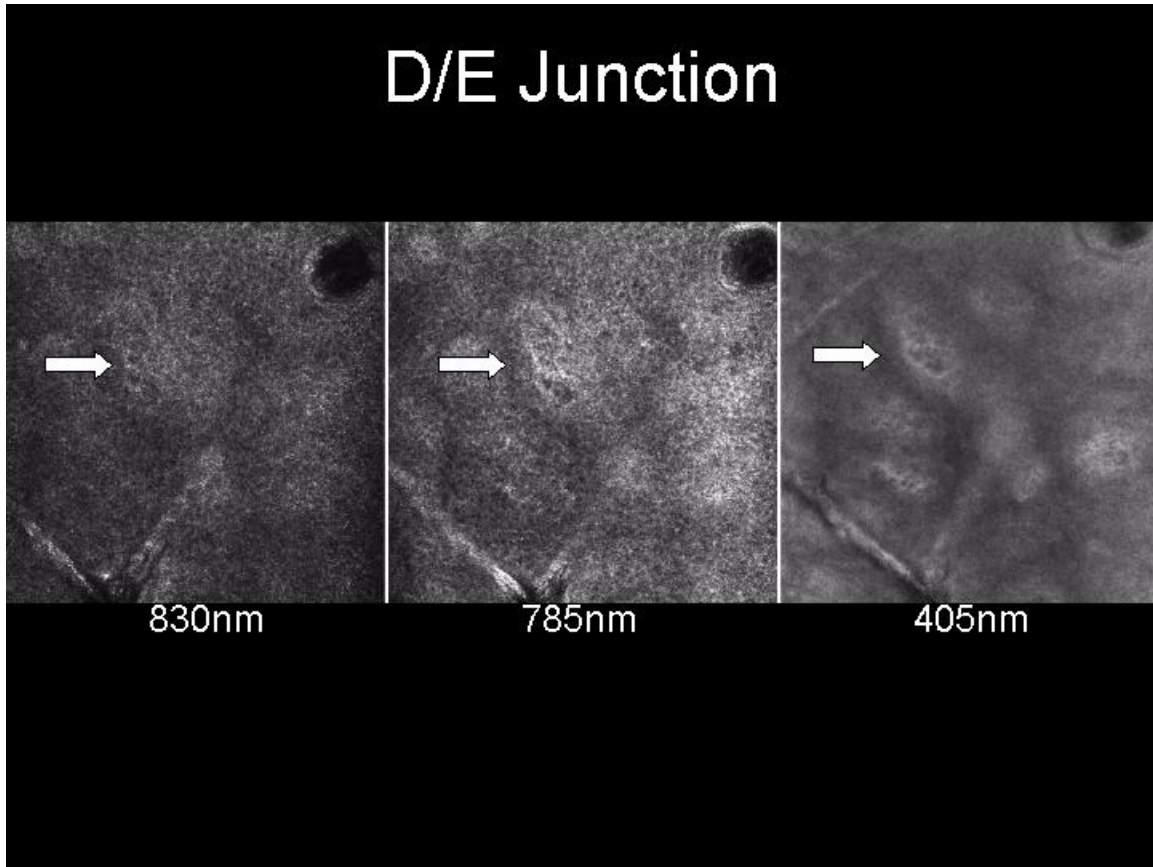
Appendix D

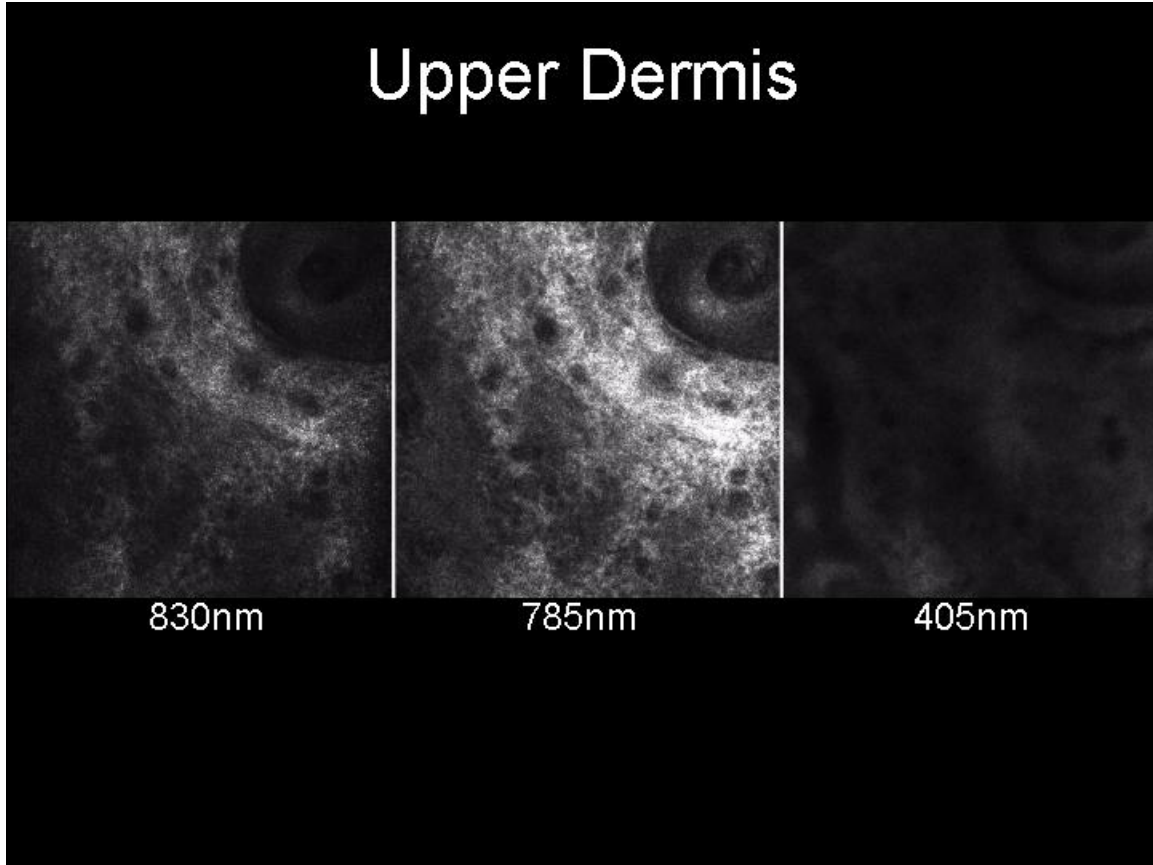
Image data from human subject J-N 01 with oil immersion media:











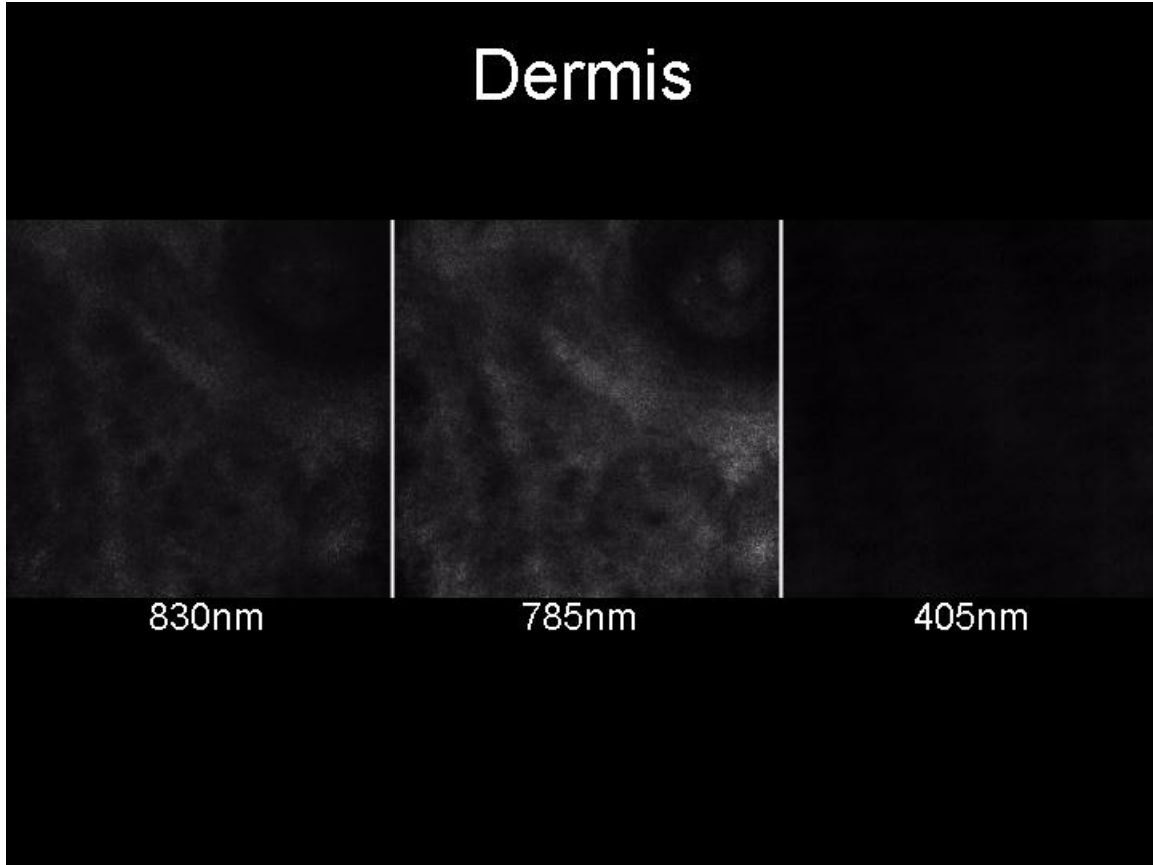
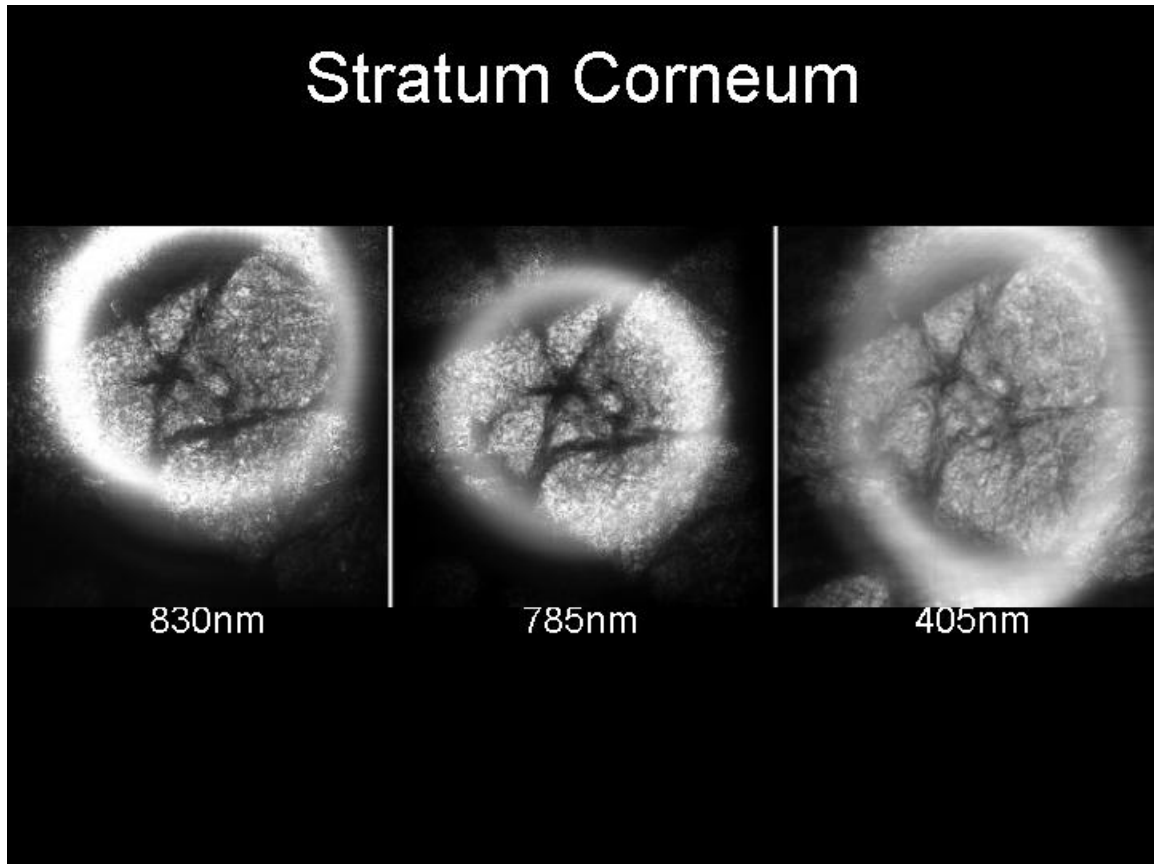
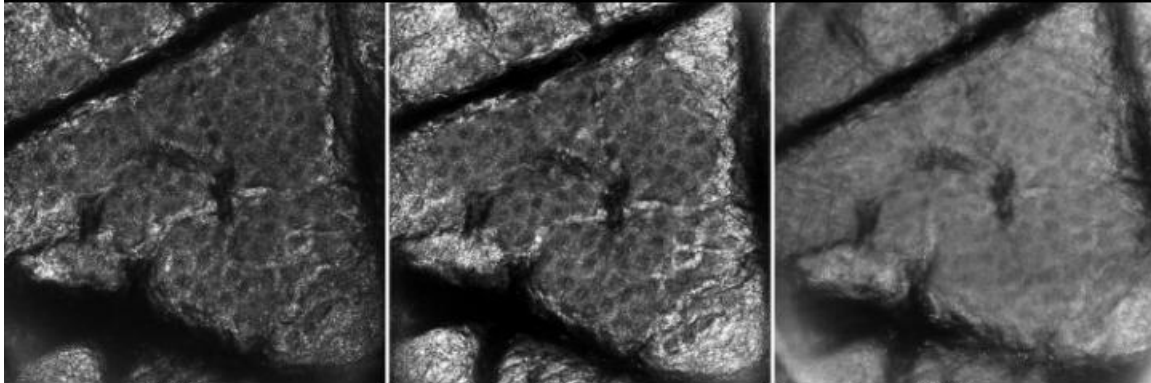


Image data from human subject PAR stack 03 with oil immersion media:



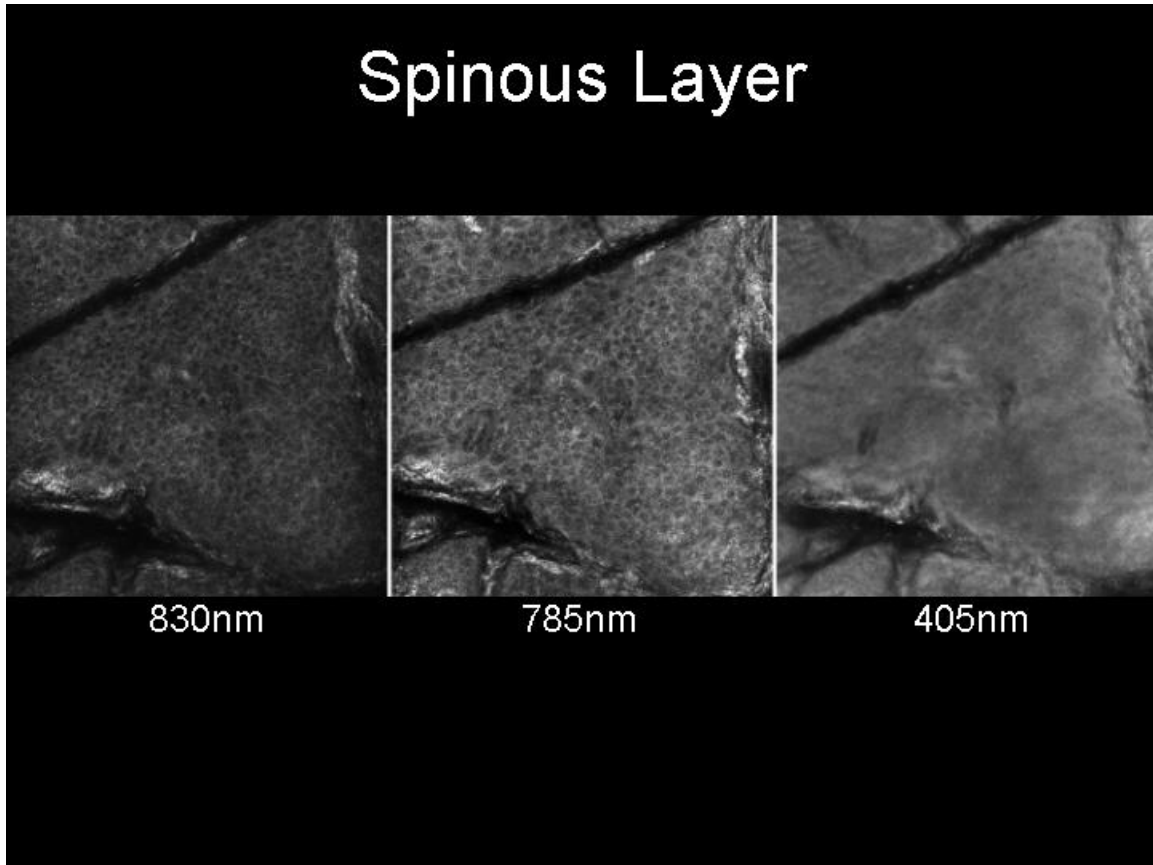
Granular Layer

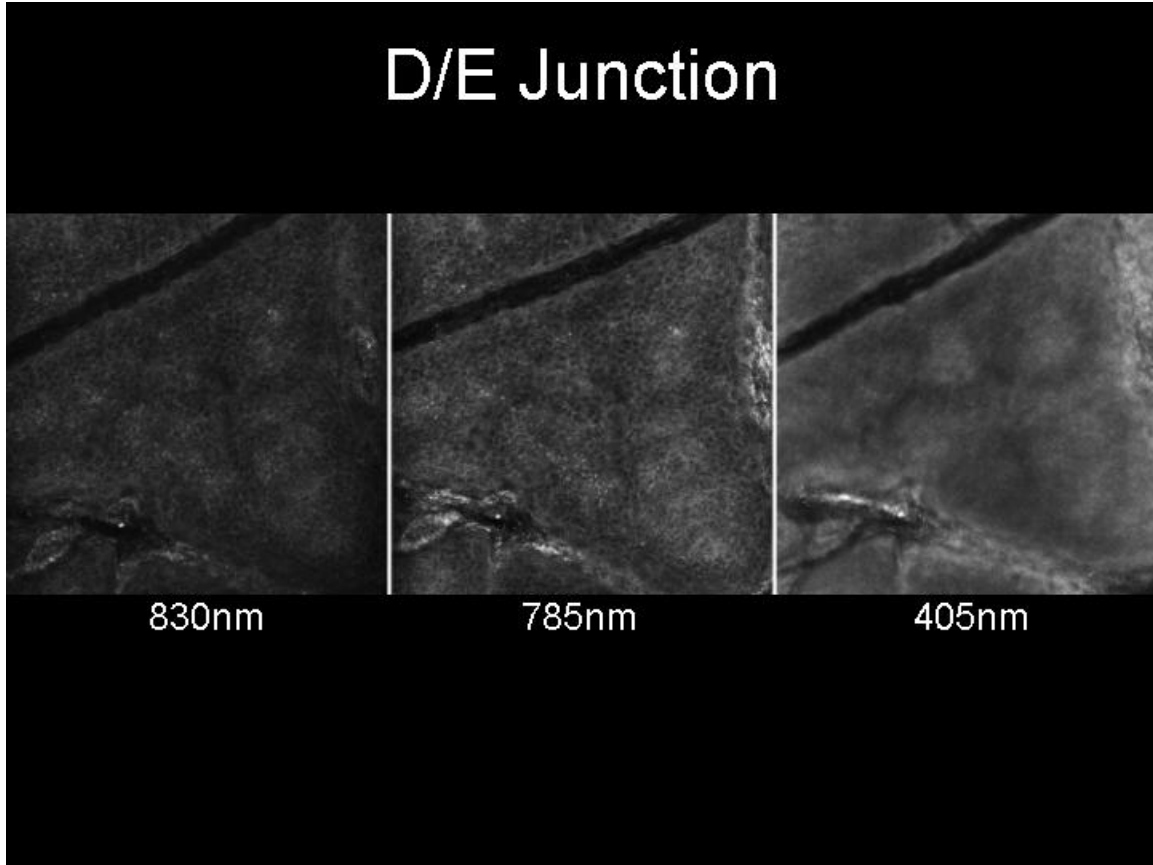


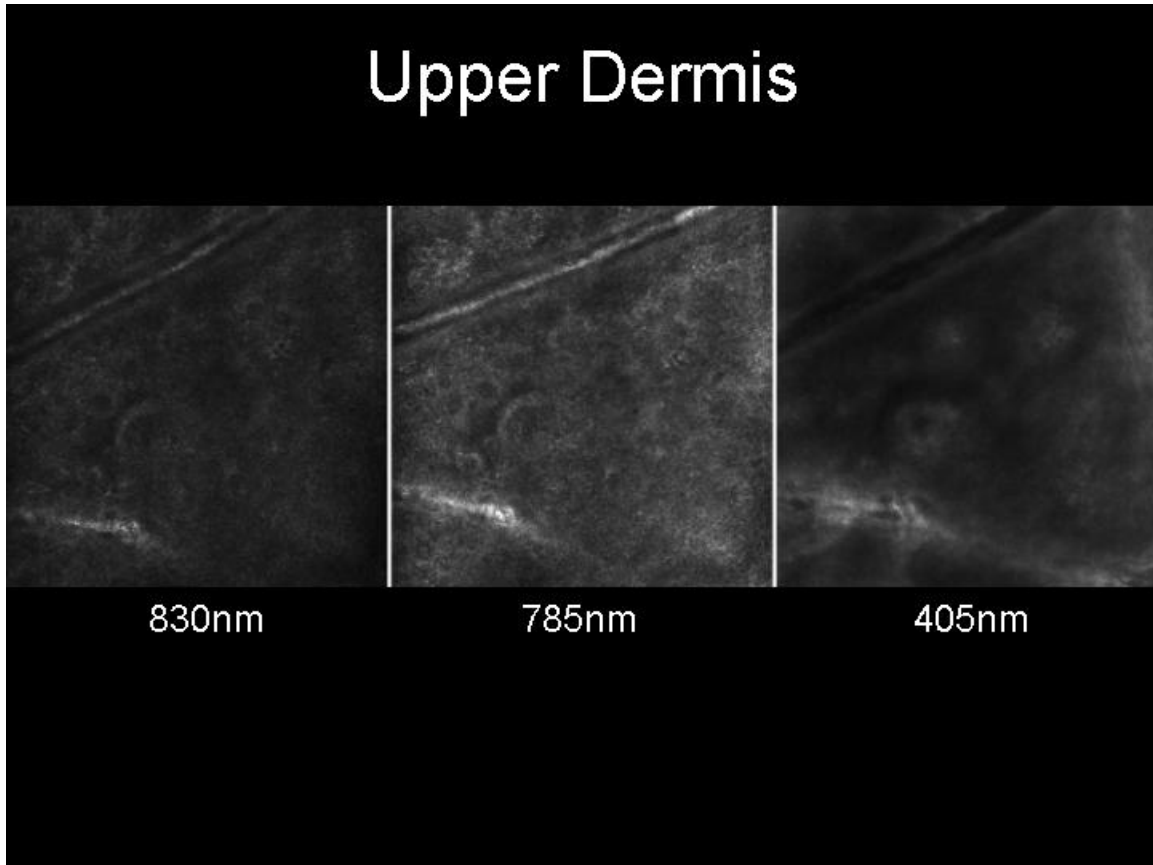
830nm

785nm

405nm







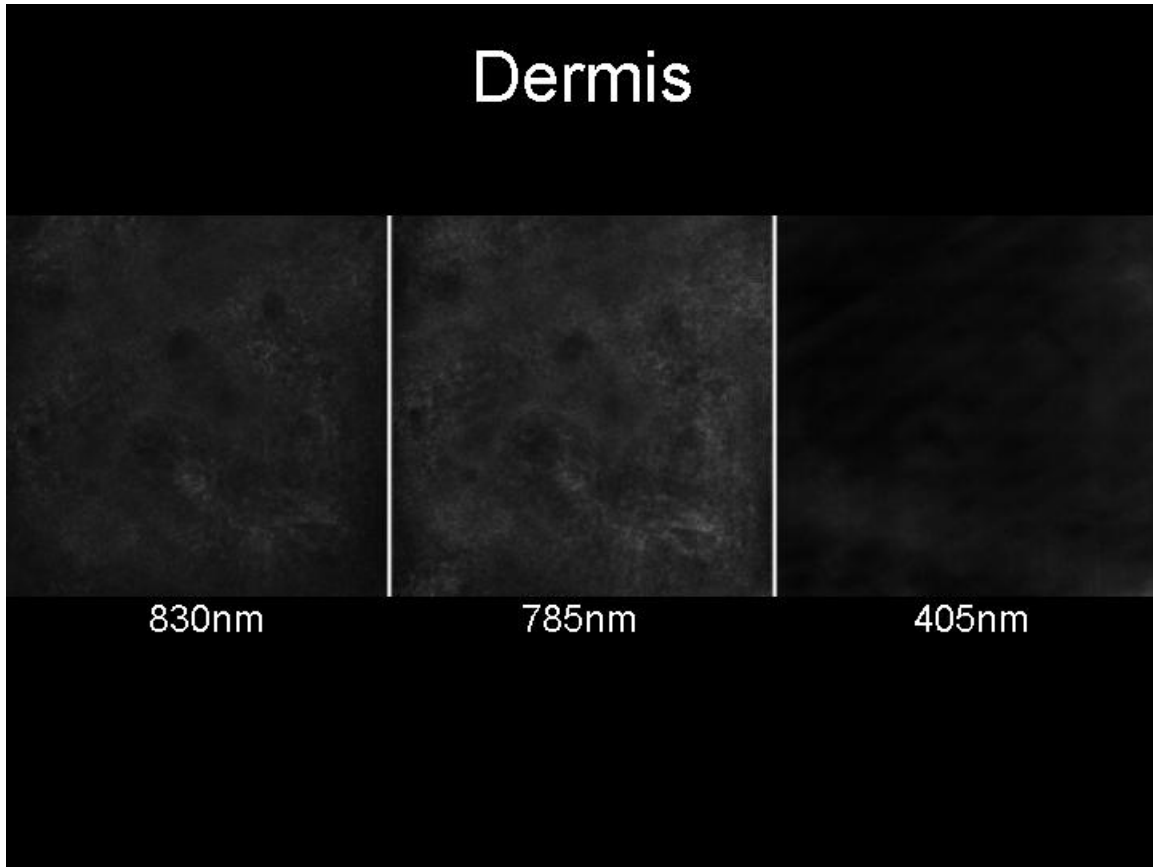
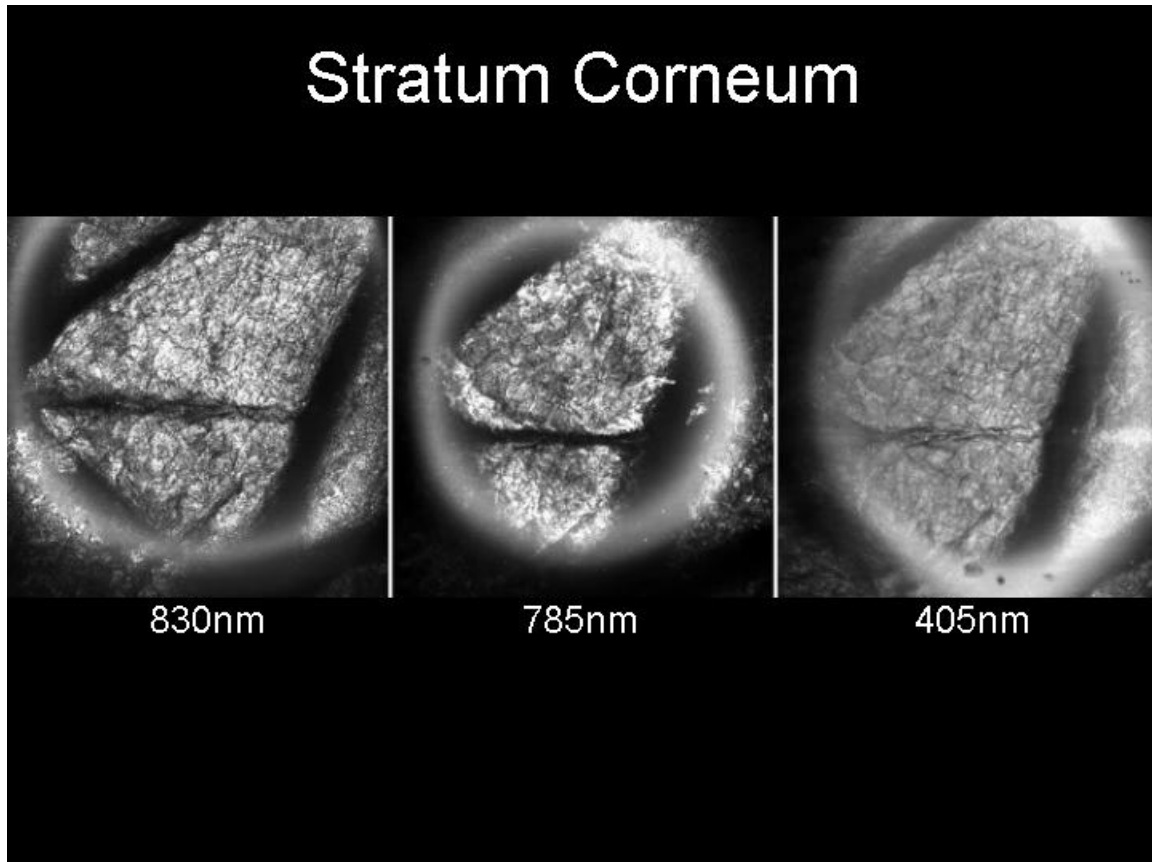
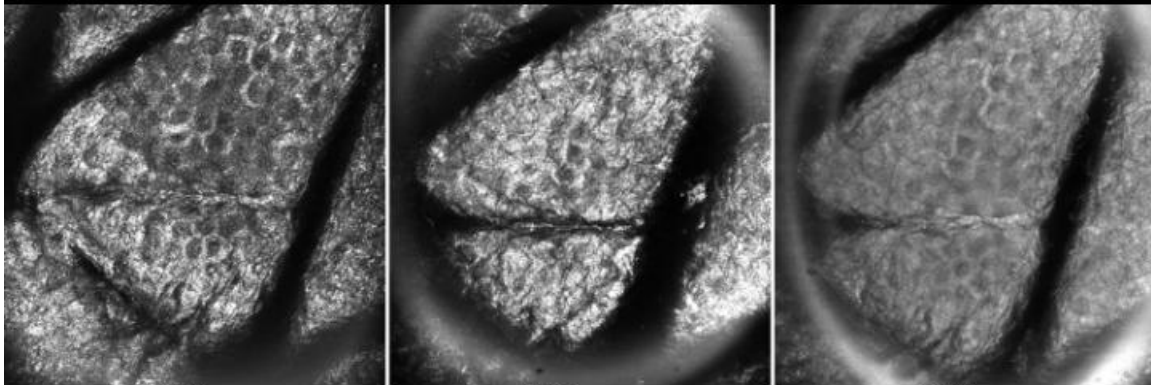


Image data from human subject SKO stack 01 with oil immersion media:



Granular Layer



830nm

785nm

405nm

